OPTIMAL FLIGHT TRAJECTORY GENERATION ALGORITHMS FOR URBAN AIR MOBILITY

Weihong Yuan

A thesis
in
The Department
of
Electrical and Computer Engineering

Presented in Partial Fulfillment of the Requirements
For the Degree of Master of Applied Science in Electrical and Computer Engineering
Concordia University
Montréal, Québec, Canada

July 2020

CONCORDIA UNIVERSITY
SCHOOL OF GRADUATE STUDIES

This is to certify that the thesis prepared

By: Weihong Yuan

Entitled: Optimal Flight Trajectory Generation Algorithms for Urban Air Mobility

and submitted in partial fulfillment of the requirements for the degree of

Master of Applied Science (Electrical and Computer Engineering)

complies with the regulations of this University and meets the accepted standards with respect to originality and quality.

Signed by the final examining committee:

_____ Chair
Dr. W. Lucia (CIISE)

_____ External Examiner
Dr. W. Lucia (CIISE)

_____ Internal Examiner
Dr. K. Skonieczny

_____ Supervisor
Dr. L. Rodrigues

Approved by: _____
Dr. Y.R. Shayan, Chair
Department of Electrical and Computer Engineering

_____ 20___ _____
Dr. Mourad Debbabi, Interim Dean,
Faculty of Engineering and Computer Science

Abstract

Optimal flight trajectory generation algorithms for urban air mobility

Weihong Yuan

The concept of Urban Air Mobility (UAM) has gained significant attention recently. In this vibrant domain, the capability of generating an optimal flight trajectory is of essential importance. This study aims to provide analytical solutions to generate the optimal trajectory in the three most common UAM scenarios. The first case is the comfort-optimal trajectory for drone package delivery and air taxis carrying passengers. The cost is evaluated as a linear combination of acceleration (or specific support force) and flight time. The second case is the control-effort-optimal trajectory for hovering vehicles. Hovering vehicles are expected to be the dominant model of air taxi. The objective function is a linear combination of thrust and flight time. The third case is the Direct-Operating-Cost (DOC) optimal trajectory for electric fixed-wing aircraft, on which all major aerospace companies are working. DOC is a linear combination of energy consumption and flight time.

The trajectory optimization problems are formulated as optimal control problems and the Pontryagen's Minimum Principle is applied to solve them. The solution is the reference position as a function of time, which is a guidance law and is fed to the downstream flight controller. The biggest advantage of an analytical solution is to reduce the computational time. It can also be integrated with other flight path planning methods. Several simulation examples will be presented to show the effectiveness of the proposed method.

Acknowledgments

I wish to express my deepest gratitude to my supervisor, Professor Luis Rodrigues, who recognized my problem-solving abilities, convincingly guided and encouraged me to be professional and do the right things even when the road got tough. Without his persistent help, the goal of this project would not have been realized.

I wish to show my gratitude to my colleagues, Bruno Carvalho, Mitchell Lichocki, Steven Li, Mailis Rodrigues, Júlia Zamboni, Maryam Bagherzade. It is whole-heartedly appreciated that your great advice for my study proved monumental towards the success of this study.

I am indebted to MITACS, Marinvent and Concordia University. Without their support and funding, this study could not have been completed.

I would like to pay my special regards to my family. They kept me going on and this work would not have been possible without their input.

I wish to thank all the people whose help was a milestone in the completion of this project.

Last but not least, I would like to recognize the invaluable assistance from Concordia staff during my study.

Contents

List of Figures

List of Tables

Chapter 1

Introduction

Recently, the concept of Urban Air Mobility (UAM) has gained significant attention. UAM enables safe and efficient air traffic operations in a metropolitan area [5] as illustrated in Fig. 1. In such future urban airspace, there are aircraft delivering packages or transporting passengers. The aircraft are of different types, such as hovering vehicles and fixed-wing. In this vibrant domain, the capability of generating an optimal flight trajectory from the origin to the destination is of essential importance. From the customer's point of view, an important question is what is the optimal flight trajectory for passenger comfort and package delivery. From the operator's point of view, an important question is what is the optimal trajectory minimizing the operating cost.

This study aims to provide analytical solutions to generate the optimal trajectory in three target scenarios. Analytical solutions not only reduce the computational time but provide physical insight as well. Additionally, they can also be integrated with other flight path planning methods.

Figure 1: UAM illustration [1]

To achieve a certain level of abstraction, so as to provide beneficial robustness in flight trajectory tracking, it is favorable to have a double layered system (Fig. 2), namely a Flight Management System (FMS) as the upper level and a Flight Control System (FCS) as the lower level. A FMS generates waypoints or continuous guidance and feeds them into the FCS, whose task is to control the aircraft to track the trajectory [6]. In this research, we work on FMS only. Note that the outputs of the FMS, such as position and attitude as a function of time, can be treated as reference inputs to the FCS. On the other hand, in most applications the dynamics of the FCS, such as speed variation for example, are fast enough to be neglected by the FMS.

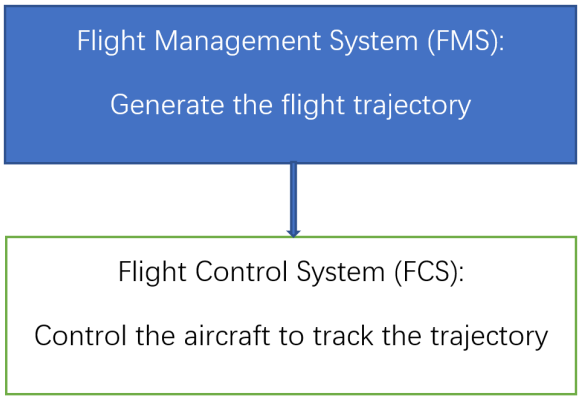

Figure 2: Layered structure of FMS-FCS

1.1 Literature Survey

Drones are more and more capable of a wide range of applications such as remote sensing, the delivery of packages and agricultural spraying [7]. Many companies are conducting research and development on delivery using drones because unmanned delivery can save costs and time since drones are not constrained by traffic jams [8]. Drone organ delivery for transplants appears naturally as a potential application because the payload is not usually very heavy, it does not take much space to be transported, and its delivery is typically an emergency [9]. Reference [10] addressed the security problem with drones for organ delivery such as hacking and privacy issues. Since the organs or any other precious and fragile parcel may be damaged by contact, friction, or collision due to the motion of the carrier, one needs to find a way to fly the carrier to minimize these damages during flight. This can be done by minimizing the dynamic force transferred to the package. Another application scenario that may appear soon in the future for the methodology proposed in this study is urban transportation and passenger comfort. Europe has adopted the Flight Path 2050 Challenge

demanding that 90 percent of travelers are able to complete their journey door-to-door within four hours by 2050 [11]. A similar concept took its shape earlier in the USA named SATS (Small Aircraft Transportation System), aiming at dealing with the saturation of existing transportation systems [12]. In this case, travel comfort and satisfaction may become the number one factor, which is strongly related to the body acceleration transferred by the aircraft to the passengers [13]. Therefore, it is essential to be able to generate an optimal flight trajectory onboard in real-time. Many trajectory generation methods have been developed, such as the sampling-based approach [14], artificial heuristic approach [15], geometry-based approach [16], BADA model-based approach [17] and dynamic programming [18], to name a few. Several articles have studied optimal flight trajectories for different objectives. References [6, 19] solved the optimal control problem for fixed-wing aircraft by splitting the flight profiles into three segments (climb, cruise, and descent) and yielding an optimal speed profile for the given (regulated) flight path. References [20–22] studied the optimal trajectory for the shortest flight time. Reference [23] provided a numerical solution of the optimal energy-efficient trajectory of a quadrotor UAV assuming that the initial and final angular velocities of each motor are identical. Reference [24] tackled the minimal acceleration trajectory for quadrotors in the 2D vertical plane, while reference [25] studied the minimal control effort trajectory in the vertical plane considering first order drag effects in one direction. In chapter 2, we present the flight trajectories that optimize the passenger comfort and the package delivery performance.

After viewing the optimal trajectory from the passenger's point of view, we continue to look at the problem from the operator's point of view in chapters 3 and 4. Since the model of the aircraft must be considered during the problem formulation, we deal with two most common models: hovering vehicles and fixed-wing aircraft. In chapter 3, we determine the flight trajectory which optimizes the control effort.

The research of optimal trajectories from the operator's point of view starts with fuel propelled fixed-wing aircraft. The authors in [26] investigated the fuel-optimal trajectory and summarized existing dynamic models to formulate the problem, which inspired our problem formulation. In chapter 3, the model of hovering vehicles will be studied as shown in Fig. 3. The articles [20, 27] studied the time-optimal trajectory for quadrotors. Feasible ranges of the control inputs were studied in [27]. Reference [24] tackled the minimal acceleration trajectory for quadrotors in a 2D vertical plane. The work presented in [28] was on snap-optimal trajectory. The research published in [29] studied the minimal control effort trajectory in the vertical plane with 1D drag. The study was performed only for zero boundary conditions taking the pitch angle and thrust as control inputs. It was claimed in the paper that a completely analytical solution was not possible. The authors in [30]

Figure 3: Hovering vehicle, passenger drone [2]

investigated a similar problem even though it was interpreted as the energy-optimal trajectory. A second order drag model was considered and some constraints on states and control inputs were incorporated. However, the problem was solved in 1D. Unfortunately, the 3D trajectory would not simply be the combination of the three decoupled 1D trajectories. Similar to [29], only the optimal control law was obtained instead of an explicit solution of the optimal trajectory. Reference [23] solved numerically the optimal trajectory for a quadrotor UAV with 16 states.

By contrast with the previous literature, the objective of chapter 3 is to analytically solve the optimal trajectory by trading-off control effort and flight time. The benefits of the result are threefold, 1) it implies a potential longer lifetime of the actuators and less maintenance cost, 2) it implies less energy consumption since control effort is directly related to energy consumption, 3) it might require less space and weight for the aircraft at an early design stage. Most published studies on trajectory generation in wind were conducted for fixed-wing aircraft. Article [31] analyzed wind effects (specifically head and tail wind) on Direct Operating Cost (DOC) optimal cruise-descent trajectories. Reference [32] extended Neighboring Optimal Control (NOC) to study the minimum-time problem for a horizontal flight in a variable wind. The work in [33] determined the fuel-optimal cruise altitude considering a zero gradient of fuel consumption rate and then the time-optimal horizontal route was computed with Dynamic Programming (DP). Candidate optimal control actions were found in [34] to minimize energy consumption for an airship straight flight in a constant

wind field. Reference [35] used network flow methods and Dijkstra's algorithm to find the shortest path while assuming a fixed airspeed and flight level. The authors in [36] applied a genetic algorithm to study flight track optimization for North Atlantic Airspace (NAT). Reference [37] represented lateral routes as a graph and calculated wind-optimal trajectories by a shortest-path search. Article [38] studied time-optimal path planning in a uniform horizontal wind for stationary flights. Another way to calculate the vertical flight cost with performance database was proposed in [39] and verified with FlightSIM and FMS benchmarks. Reference [40] used a genetic algorithm to select the optimal speeds, altitudes and wind for a fuel-optimal trajectory, while Dijkstra's algorithm was used in [41] to compute the fuel-optimal route through a 3D fixed flight network consisting of discrete waypoints. The authors in [42] studied the optimal vertical descent route in presence of along-track and cross wind, while assuming idle thrust. The work in [43] obtained the optimal trajectory with parametric optimization. Reference [44] proposed a narrower new trans-Atlantic route structure to take advantage of wind, specifically jet streams. Reference [45] studied the energy-optimal cruise direction of a multirotor given a constant speed. Reference [46] studied a time-optimal path for a quadrotor while assuming a constant airspeed. In [47], global optimization was broken into three smaller problems: waypoint optimization, jerk-optimal interpolation and time-optimal adaption. Reference [48] applied swarm particle optimization to follow trajectories with more favorable wind. Article [49] computed the time-optimal trajectory using Bellman's algorithm on a wind grid. The authors of [50] found a fuel-optimal path for the descent and approach phase with a combination of optimal control and a modified A* algorithm. Study [51] showed differences in fuel consumption caused by the differences between forecast and actual wind data. The work in [52] used a Radau pseudospectral method to generate the trajectory in both steady uniform and boundary-layer wind fields.

A bright future for aviation with less emission, lower noise levels and higher operating efficiency was opened by electric aircraft, such as the Airbus E-fan [53] depicted in Fig 4. An essential functionality in demand is performance-optimal trajectory [54] onboard generation. The authors of [55] conducted a comprehensive review of multi-objective flight trajectory optimization techniques. Reference [56] reviewed system modeling and optimization methods for an air traffic management system. Another recent review on mathematical modeling and objective functions for trajectory optimization was presented in [57]. Paper [58] studied climb and descent trajectories using the energy-state approximation. Thrust was considered as a function of speed and altitude for some cases. The result was a control law of speed and altitude for each value of the energy-state. Article [26] summarized various aircraft models to formulate the optimization problem and selected also the energy-state model to address

Figure 4: Airbus E-fan [3]

fuel-minimum and time-minimum trajectories, respectively. Thrust and path angle were chosen as the control variables. Maximum thrust for climb, steady cruise, and minimum thrust for descent were assumed. The work in [59] investigated the DOC-optimal longitudinal path for a short-haul flight using the energy-state equations. Effects of horizontal along-track wind were also included. Reference [60] surveyed and summarized the studies on the DOC-optimal longitudinal path up to the 1980s. The energy-state methods inspired us treating the horizontal position as the independent variable instead of time. Paper [61] examined the impact of the procedural constraints (such as maximum thrust climb, steady cruise, and minimum thrust descent) on the total cost while assuming a constant mass. The authors claimed that if the fuel consumption is independent of thrust, constrained thrust trajectories gave identical performance to free thrust trajectories in terms of fuel consumption. Note that the constant mass assumption is verified by electric aircraft. Article [62] investigated the fuel-optimal longitudinal path with a point mass model using Pontryagin's Minimum Principle (PMP) and singular perturbation theory. Reference [63] explored the fuel-optimal climb-out considering turning. It was claimed that decoupling turning and climbing was more efficient than simultaneously turning and climbing. Hence, we only deal

with the longitudinal flight in this study. The fuel-optimal longitudinal path to absorb delay in presence of altitude-dependent horizontal wind was studied in [31]. The authors of [6] considered the DOC-optimal vertical path by applying PMP to each phase individually. For example, when dealing with the climb phase, the terminal cost was approximated with the cruise cost rate and the estimated cruise time. The shooting method was used to find the optimal speed. The DOC-optimal cruise for electric aircraft was addressed in [64]. Article [18] used lift coefficient and thrust as inputs and applied Dynamic Programming (DP) to solve the fuel-optimal vertical route. Collocation methods were used in [65, 66] to compute the optimal vertical trajectory. In each phase, one procedure constraint was enforced such as constant airspeed climb, constant altitude cruise, and constant Mach number descent. The solution was verified with backward integration of the computed terminal states and costates to recover the initial values. Both the vertical and horizontal paths were addressed in [66]. Reference [67] applied a pseudospectral collocation method. More details on collocation methods can be found in [68, 69]. Paper [39] provided an example of parameterization and heuristic methods for trajectory generation. A genetic algorithm was presented in [70] to find the fuel-optimal speed and altitude for a vertical flight. Paper [71] applied hybrid optimal control (HOC) to find the fuel-optimal vertical path. The control input was throttle. The trajectory was split into three phases and in each phase a constraint was imposed such as climb throttle in climb, constant altitude cruise and idle throttle in descent. An indirect numerical method was developed and the result was the bang-singular-bang solution. A set of initial guesses were required for the solution.

Overall, Table 1 collects what is missing in the open literature for the three defined problems.

Table 1: Missing points in open literature

Scenarios	Literature	Missing points
Problem 1	[7]-[25]	3D analytical solution for arbitrary boundary conditions, explicit formula for the cost
Problem 2	[26]-[52]	3D analytical solution for arbitrary boundary conditions in a wind field
Problem 3	[53]-[72]	Optimal solution for all phases of flight in a wind field

The structure of this thesis is as follows. Chapter 2 presents the flight trajectory that optimizes the passenger comfort or package delivery performance. In chapter 3, we provide the trajectory that optimizes the control effort and flight time for hovering vehicles. The trajectory that optimizes the energy consumption and flight time for electric fixed-wing aircraft is found in chapter 4. Concluding remarks are stated in chapter 5.

1.2 Contributions

The contributions of this thesis are optimal trajectory solutions to the following three problems:

Problem 1: Optimal trajectory for passenger comfort and package delivery

- The proposed solution determines the optimal trajectory in three-dimensional space for arbitrary feasible initial and terminal conditions. An explicit formula for the cost is obtained and a peak velocity constraint is enforced.
- The algorithm can be implemented in common embedded processors since it is designed to use simple calculations no harder than square root and division operations.

Problem 2: Optimal trajectory trading-off control effort and flight time for hovering vehicles

- The proposed approach can find the analytical solution for either a fixed time or a free time. Additionally, for long haul flights, an approximate solution is presented to reduce the computational time. A characteristic parameter is proposed to decide whether to use the analytical solution or the approximation.
- The approach is extended to satisfy peak velocity constraints.
- The optimal trajectory in a constant wind shear field is derived while respecting peak thrust constraints.

Problem 3: DOC-optimal trajectory for electric fixed-wing aircraft

- The trajectory planning is formulated as a hybrid optimal control problem (HOCP) to find the optimal trajectory for all phases of flight.
- The proposed solution does not require an initial guess of the costate, which saves computational time.
- Altitude-dependent along-track wind is considered so that the optimal flight profile in the presence of wind can be found.
- A maximum Mach number constraint and a maximum lift coefficient constraint are enforced in a suboptimal solution to prevent results that are practically infeasible.

Chapter 2

Onboard Generation of Optimal Flight Trajectory for Package Delivery and Passenger Comfort

2.1 Introduction

In this chapter, we present the flight trajectory which optimizes the passenger comfort. The contributions of this chapter are:

- the proposed solution yields the optimal trajectory in three-dimensional space for arbitrary feasible initial and terminal conditions,
- an explicit formula for the cost is obtained and a peak velocity constraint is enforced,
- the algorithm can be implemented in common embedded processors since it is designed to use simple calculations no harder than square root and division operations.

The structure of this chapter is as follows. Preliminary information on optimal flight modes and the detailed solution of the optimal control problem in 3D space are presented in section 2.2. Simulation results are provided in section 2.3. Concluding remarks are stated in section 2.4.

2.2 Optimal Trajectory

2.2.1 Optimal Flight Modes

The first step of trajectory optimization is to decide on the functional to be optimized. The most common are:

- Minimum time of flight,
- Maximum endurance,
- Maximum range,
- Economy mode (ECON): Minimization of the direct operating cost of flight, which is a trade-off between the cost of energy and time-related costs,
- Optimal fragile package delivery: Minimization of a linear combination of flight time and dynamic force,
- Optimal passenger satisfaction: Minimization of a linear combination of flight time and total acceleration.

We will focus on the last two optimization problems.

2.2.2 Optimal Control Problem

To formulate our problem we define the state of the aircraft as $x = [p_1, p_2, p_3, v_1, v_2, v_3]^T$, where p_i are the position coordinates and v_i are the velocity coordinates for $i = 1, 2, 3$. The aircraft dynamics are described by

$$\begin{bmatrix} \dot{p_1} \\ \dot{p_2} \\ \dot{p_3} \\ \dot{v_1} \\ \dot{v_2} \\ \dot{v_3} \end{bmatrix} = \begin{bmatrix} 0 & 0 & 0 & 1 & 0 & 0 \\ 0 & 0 & 0 & 0 & 1 & 0 \\ 0 & 0 & 0 & 0 & 0 & 1 \\ 0 & 0 & 0 & 0 & 0 & 0 \\ 0 & 0 & 0 & 0 & 0 & 0 \\ 0 & 0 & 0 & 0 & 0 & 0 \end{bmatrix} \begin{bmatrix} p_1 \\ p_2 \\ p_3 \\ v_1 \\ v_2 \\ v_3 \end{bmatrix} + \begin{bmatrix} 0 & 0 & 0 \\ 0 & 0 & 0 \\ 0 & 0 & 0 \\ 1 & 0 & 0 \\ 0 & 1 & 0 \\ 0 & 0 & 1 \end{bmatrix} \begin{bmatrix} u_1 \\ u_2 \\ u_3 - g \end{bmatrix} \tag{1}$$

As discussed in Chapter 1, the terms that matter in this problem are specific force (acceleration) and flight time. This is the reason why the double integrator is a good model. We define the running cost $L(u) = 0.5u^T u + C_I$, where $C_I(m^2/s^4)$ is called the cost index, which is the ratio of the cost of one time unit to the cost of one unit of acceleration. Our optimal control problem is then formulated as

$$\begin{aligned} J = \min_u \quad & \int_0^{t_f} L(u)dt \\ s.t. \quad & \dot{x} = f(x, u) \\ & x(0) = x_0, x_f \text{ given} \\ & u \in \Omega \end{aligned} \tag{2}$$

where x is the state of the aircraft, $f(x,u)$ is the vector field representing the dynamics (1), Ω is the admissible set of inputs u, and t_f is the flight time.

The solution of this problem will be obtained using the Pontryagin's Minimum Principle (PMP) [73, 74]. Writing the optimal control as $u^*(t)$, and the optimal trajectory as $x^*(t)$, we define

$$\lambda = \frac{\partial J}{\partial x^*} \tag{3}$$

$$H = L(u^*) + \lambda^T f(x^*, u^*) \tag{4}$$

Then the necessary conditions (NC) for a minimizer are

$$\frac{\partial H}{\partial u} = 0 \tag{5}$$

$$\frac{\partial H}{\partial x} = -\dot{\lambda} \tag{6}$$

We are now ready to present the main result.

Theorem 2.2.1 *The optimal flight trajectory is*

$$p(t) = \begin{bmatrix} \frac{C_1}{6}t^3 - \frac{C_4}{2}t^2 + C_{10}t + C_7 \\ \frac{C_2}{6}t^3 - \frac{C_5}{2}t^2 + C_{11}t + C_8 \\ \frac{C_3}{6}t^3 - \frac{Cg_6}{2}t^2 + C_{12}t + C_9 \end{bmatrix} \tag{7}$$

where

$$\begin{bmatrix} C_1 \\ C_2 \\ C_3 \end{bmatrix} = \frac{6}{t_f^3} \begin{bmatrix} (v_1(0) + v_1(t_f))t_f + 2(p_1(0) - p_1(t_f)) \\ (v_2(0) + v_2(t_f))t_f + 2(p_2(0) - p_2(t_f)) \\ (v_3(0) + v_3(t_f))t_f + 2(p_3(0) - p_3(t_f)) \end{bmatrix}$$

$$\begin{bmatrix} C_4 \\ C_5 \\ Cg_6 \end{bmatrix} = \frac{2}{t_f^2} \begin{bmatrix} (2v_1(0) + v_1(t_f))t_f + 3(p_1(0) - p_1(t_f)) \\ (2v_2(0) + v_2(t_f))t_f + 3(p_2(0) - p_2(t_f)) \\ (2v_3(0) + v_3(t_f))t_f + 3(p_3(0) - p_3(t_f)) \end{bmatrix} \tag{8}$$

$$[C_7, C_8, C_9, C_{10}, C_{11}, C_{12}] = [p_1(0), p_2(0), p_3(0), v_1(0), v_2(0), v_3(0)]$$

the optimal acceleration due to dynamic forces is

$$u^*(t) = \begin{bmatrix} C_1 t - C_4 \\ C_2 t - C_5 \\ C_3 t + g - Cg_6 \end{bmatrix} \tag{9}$$

and the optimal cost is

$$\begin{aligned} J = \left(C_I + \frac{1}{2}g^2\right) t_f + g\,(v_{3f} - v_{30}) + \sum_{i=1}^{3} \left[2(v_{i0}^2 + v_{if}^2 + v_{i0}v_{if})t_f^{-1}\right. \\ \left. + 6(v_{i0} + v_{if})(p_{i0} - p_{if})t_f^{-2} + 6(p_{i0} - p_{if})^2 t_f^{-3}\right] \end{aligned} \tag{10}$$

where v_{if}, v_{i0} stand for the final and initial velocity in the ith direction, respectively, and $i = 1, 2, 3$.

Proof: The Hamiltonian is

$$H = \frac{1}{2}u^T u + \begin{bmatrix} \lambda_1 \\ \lambda_2 \\ \lambda_3 \end{bmatrix}^T \begin{bmatrix} \dot{p}_1 \\ \dot{p}_2 \\ \dot{p}_3 \end{bmatrix} + \begin{bmatrix} \lambda_4 \\ \lambda_5 \\ \lambda_6 \end{bmatrix}^T \begin{bmatrix} \dot{v}_1 \\ \dot{v}_2 \\ \dot{v}_3 \end{bmatrix} + C_I \tag{11}$$

From (1) and (5),

$$\frac{\partial H}{\partial u} = \begin{bmatrix} u_1 \\ u_2 \\ u_3 \end{bmatrix} + \begin{bmatrix} \lambda_4 \\ \lambda_5 \\ \lambda_6 \end{bmatrix} = \begin{bmatrix} 0 \\ 0 \\ 0 \end{bmatrix} \tag{12}$$

$$u^* = [-\lambda_4, -\lambda_5, -\lambda_6]^T \tag{13}$$

The optimal Hamiltonian is

$$H^* = -\frac{1}{2}(\lambda_4^2 + \lambda_5^2 + \lambda_6^2) + \lambda_1 v_1 + \lambda_2 v_2 + \lambda_3 v_3 - \lambda_6 g + C_I \tag{14}$$

From (6) we obtain

$$\frac{\partial H}{\partial p} = \begin{bmatrix} 0 \\ 0 \\ 0 \end{bmatrix} = \begin{bmatrix} -\dot{\lambda}_1 \\ -\dot{\lambda}_2 \\ -\dot{\lambda}_3 \end{bmatrix}, \frac{\partial H}{\partial v} = \begin{bmatrix} \lambda_1 \\ \lambda_2 \\ \lambda_3 \end{bmatrix} = \begin{bmatrix} -\dot{\lambda}_4 \\ -\dot{\lambda}_5 \\ -\dot{\lambda}_6 \end{bmatrix} \tag{15}$$

$$[\lambda_1, \lambda_2, \lambda_3] = [C_1, C_2, C_3] \tag{16}$$

$$\begin{bmatrix} \lambda_4 \\ \lambda_5 \\ \lambda_6 \end{bmatrix} = \begin{bmatrix} -C_1 t + C_4 \\ -C_2 t + C_5 \\ -C_3 t + C_6 \end{bmatrix} \tag{17}$$

From (1) we know that

$$\dot{p} = v$$

$$\dot{v} = \begin{bmatrix} u_1 \\ u_2 \\ u_3 - g \end{bmatrix} = \begin{bmatrix} -\lambda_4 \\ -\lambda_5 \\ -\lambda_6 - g \end{bmatrix} = \begin{bmatrix} C_1 t - C_4 \\ C_2 t - C_5 \\ C_3 t - C_6 - g \end{bmatrix} \tag{18}$$

Define

$$Cg_6 = C_6 + g \tag{19}$$

Integrating equation (18) yields

$$v = \begin{bmatrix} \frac{C_1}{2}t^2 - C_4 t + C_{10} \\ \frac{C_2}{2}t^2 - C_5 t + C_{11} \\ \frac{C_3}{2}t^2 - Cg_6 t + C_{12} \end{bmatrix} \tag{20}$$

$$p = \begin{bmatrix} \frac{C_1}{6}t^3 - \frac{C_4}{2}t^2 + C_{10}t + C_7 \\ \frac{C_2}{6}t^3 - \frac{C_5}{2}t^2 + C_{11}t + C_8 \\ \frac{C_3}{6}t^3 - \frac{Cg_6}{2}t^2 + C_{12}t + C_9 \end{bmatrix} \tag{21}$$

which is the same result as (7). The boundary conditions are

$$[p_1(0), p_2(0), p_3(0), v_1(0), v_2(0), v_3(0)]^T = [C_7, C_8, C_9, C_{10}, C_{11}, C_{12}]^T \tag{22}$$

$$\begin{bmatrix} p_1(t_f) \\ p_2(t_f) \\ p_3(t_f) \\ v_1(t_f) \\ v_2(t_f) \\ v_3(t_f) \end{bmatrix} = \begin{bmatrix} \frac{C_1}{6}t_f^3 - \frac{C_4}{2}t_f^2 + C_{10}t_f + C_7 \\ \frac{C_2}{6}t_f^3 - \frac{C_5}{2}t_f^2 + C_{11}t_f + C_8 \\ \frac{C_3}{6}t_f^3 - \frac{Cg_6}{2}t_f^2 + C_{12}t_f + C_9 \\ \frac{C_1}{2}t_f^2 - C_4 t_f + C_{10} \\ \frac{C_2}{2}t_f^2 - C_5 t_f + C_{11} \\ \frac{C_3}{2}t_f^2 - Cg_6 t_f + C_{12} \end{bmatrix} \tag{23}$$

Solving the set of equations (22) and (23), with respect to the constants $C_i, i = 1, \ldots, 12$, yields (8). According to (2) and (9), the optimal cost is

$$\begin{aligned} J &= \int_0^{t_f} \frac{1}{2} \begin{bmatrix} C_1 t - C_4 \\ C_2 t - C_5 \\ C_3 t - C_6 \end{bmatrix}^T \begin{bmatrix} C_1 t - C_4 \\ C_2 t - C_5 \\ C_3 t - C_6 \end{bmatrix} + C_I dt \\ &= \frac{C_1^2 + C_2^2 + C_3^2}{6} t_f^3 - \frac{C_1 C_4 + C_2 C_5 + C_3 C_6}{2} t_f^2 + \left(\frac{C_4^2 + C_5^2 + C_6^2}{2} + C_I \right) t_f \end{aligned} \tag{24}$$

Using (8) and (19) into (24) yields the optimal cost. Q.E.D.

Theorem 2.2.2 *There is at least one flight time that corresponds to a stationary point of the optimal cost. All candidates to optimal flight time are the real positive solutions of*

$$at_f^4 + ct_f^2 + dt_f + e = 0 \tag{25}$$

for which

$$4at_f^3 + 2ct_f + d = t_f \left(4at_f^2 + 2c \right) + d > 0 \tag{26}$$

where

$$\begin{aligned} a &= \left(C_I + \frac{1}{2}g^2\right) \\ c &= -2\sum_{i=1}^{3}(v_{i0}^2 + v_{if}^2 + v_{i0}v_{if}) \\ d &= -12\sum_{i=1}^{3}(v_{i0} + v_{if})(p_{i0} - p_{if}) \\ e &= -18\sum_{i=1}^{3}(p_{i0} - p_{if})^2 \end{aligned} \tag{27}$$

Proof: To calculate the optimal flight time, we compute

$$\begin{aligned} \frac{dJ}{dt_f} = \left(C_I + \frac{1}{2}g^2\right) - t_f^{-4}\sum_{i=1}^{3}[2(v_{i0}^2 + v_{if}^2 + v_{i0}v_{if})t_f^2 \\ +12(v_{i0} + v_{if})(p_{i0} - p_{if})t_f + 18(p_{i0} - p_{if})^2] \end{aligned} \tag{28}$$

and equate it to zero. Since J is class C^∞ for $t_f \in (0, +\infty)$,

$$\lim_{t_f \to 0}\frac{dJ}{dt_f} = -\infty < 0, \lim_{t_f \to +\infty}\frac{dJ}{dt_f} = \left(C_I + \frac{1}{2}g^2\right) > 0 \tag{29}$$

then J is guaranteed to have at least one stationary point. To find the stationary points of J we must solve

$$\frac{dJ}{dt_f} = 0, \text{where } t_f > 0 \tag{30}$$

Let us define

$$F = t_f^4\frac{dJ}{dt_f} = at_f^4 + ct_f^2 + dt_f + e \tag{31}$$

and

$$G = \frac{dF}{dt_f} = 4at_f^3 + 2ct_f + d = t_f\left(4at_f^2 + 2c\right) + d \tag{32}$$

We see that, $a > 0, c \leq 0$ and $e \leq 0$. The term d can be zero, positive or negative depending on the initial and terminal conditions. A necessary condition of optimality is $F = 0$, which is equation (25). A sufficient condition for a minimum is $G > 0$, or inequality (26), which finishes the proof. Q.E.D.

Remark 2.2.3 *For the optimal passenger satisfaction trajectory, the same methodology can be used with* $g = 0$.

2.2.3 On-board solution for optimal flight time

The optimal flight times are the real positive solutions of the equation (25) for which inequality (26) is verified. However, some embedded processors are incapable of solving quartic or cubic equations, complex valued arithmetic, or cubic root calculations. In this section we propose to apply the Newton-Raphson's (NR) method to find the optimal flight time t_f, which requires no harder than a division operation, since the derivative of each function is pre-determined and can be represented using the boundary conditions. The $sqrt(.)$ operation is possibly supported in most processors but, otherwise, this can also be replaced by a Newton-Raphson's iteration. The Newton-Raphson's method can fail in the following cases [75]:

- If the initial point is outside the basin of attraction for a root the algorithm may converge to another root,
- If the root is near an inflection point, i.e. $f''(x) = 0$, the iteration may diverge or oscillate, but may also converge,
- If the gradient is too small at a point, the next point may end up in another basin of attraction or even out of the domain,
- If there is oscillation near a local extremum, which then results in one of the previous cases.

In our case, to find the unique positive root of the 4th order polynomial (31), the potential failures described above can be mitigated if the initial point t^0 is chosen within the zone of attraction of each target root without any inflection point or local extremum located nearby. One can then find the optimal flight time using the following pseudocode:

Algorithm 1 finding the optimal flight time

if $d > 0$ **then**
  $t = 0$;
  $t_1 = \sqrt{-c/6}$;
  if $G(t_1) < 0$ **then**
    $t_2 = NR(G, 0)$;
    $t_3 = NR(G, t_1 + 1)$;
    if $F(t_2)F(t_3) < 0$ **then**
      $t_4 = NR(F, 0)$;
      $t_5 = NR(F, t_3 + 1)$;
      if $J(t_4) < J(t_5)$ **then**
        $t = t_4$;
      else
        $t = t_5$;
      end if
    end if
  end if
end if
if $t = 0$ **then**
  $t_1 = 1$;
  while $F(t_1) < 0$ **do**
    $t_1 = 2t_1$;
  end while
  $t = NR(F, t_1)$;
end if
return t;

where $t = NR(F, t^*)$ is a routine to find the zero-crossing point of function F in the neighborhood of t^*, defined as

Algorithm 2 Newton-Raphson's method

function NR(F, t^0)
  $t^{k-1} = t^0 - 2\epsilon; t^k = t^0;$
  while $|t^k - t^{k-1}| > \epsilon$ **do**
    $t^{k-1} = t^k;$
    $t^k = t^k - \frac{F(t^k)}{G(t^k)};$
  end while
  return $t^k;$
end function

where G is the derivative of function F, ϵ is a parameter of termination criterion.

2.2.4 Feasible flight time satisfying a peak velocity constraint

The optimal flight time from Theorem 2.2.2 is valid for unconstrained trajectories, which is usually acceptable for waypoint navigation on shorter haul flights. For longer haul flights multiple constraints should be considered. This subsection deals with the optimal trajectory with constrained peak velocity, which is the most common and practical limitation during flight, described as

$$v(t)^2 \leq V_{max}^2 \tag{33}$$

According to (20),

$$R := \sum_{i=1}^{3} \frac{C_i^2}{4} t^4 - C_i C_{i+3} t^3 + (C_{i+3}^2 + C_i C_{i+9}) t^2 - 2C_{i+3} C_{i+9} t + C_{i+9}^2 \leq V_{max}^2 \tag{34}$$

where $C_i, i = 1, \ldots, 12$, are given by (8) and Cg_6 is renamed as C_6 for convenience. Define,

$$\begin{aligned} \bar{a} &= \sum_{i=1}^{3} C_i^2 \\ \bar{b} &= -\sum_{i=1}^{3} 3C_i C_{i+3} \\ \bar{c} &= \sum_{i=1}^{3} 2(C_{i+3}^2 + C_i C_{i+9}) \\ \bar{d} &= -\sum_{i=1}^{3} 2C_{i+3} C_{i+9} \end{aligned} \tag{35}$$

so that

$$L = \frac{dR}{dt} = \bar{a}t^3 + \bar{b}t^2 + \bar{c}t + \bar{d} \tag{36}$$

and

$$K = \frac{dL}{dt} = 3\bar{a}t^2 + 2\bar{b}t + \bar{c} \tag{37}$$

The discriminant of the cubic function L is defined as

$$\Delta = 18\bar{a}\bar{b}\bar{c}\bar{d} - 4\bar{b}^3\bar{d} + \bar{b}^2\bar{c}^2 - 4\bar{a}\bar{c}^3 - 27\bar{a}^2\bar{d}^2 \tag{38}$$

The peak value of R is analyzed in the following four cases:

1. $\bar{a} = 0, \sum_{i=1}^{3} C_{i+3}^2 = 0$.
   Then $C_i = 0, C_{i+3} = 0, \forall i \in \{1, 2, 3\}, R = \sum_{i=1}^{3} C_{i+9}^2 = const.$ An example is shown in Fig. 5a.

2. $\bar{a} = 0, \sum_{i=1}^{3} C_{i+3}^2 \neq 0$.
   Then $R = \sum_{i=1}^{3} C_{i+3}^2 t^2 - 2C_{i+3}C_{i+9}t + C_{i+9}^2$, which is a convex quadratic polynomial. The peak value within a closed interval $[0, t_f]$ is always at the boundary. An example is shown in Fig. 5b.

3. $\bar{a} \neq 0, \Delta \leq 0$.
   When $\Delta < 0$, the function L has only one real root. Therefore, the function R has only one stationary point which must be a minimum because $\bar{a} > 0$. The maximum value of R is thus located at one of the boundary points of the time interval. When $\Delta = 0$, the function L has a multiple root and all of its roots are real. If L has a triple root then there is only one stationary point of R and we fall in the case already described above. If there is a double root and a single root then there are two stationary points of R. Since $\bar{a} > 0$ then for large enough values of $|t|$ the function R must grow large. Therefore neither of the two stationary points can be a maximum, which must be located at one of the boundary points of the time interval. An example is shown in Fig. 5c.

4. $\bar{a} \neq 0, \Delta > 0$.
   In this case there are three distinct real roots of L and therefore there could be a maximum of R inside the interval $[0, t_f]$. Since $\Delta > 0$, this guarantees that $\bar{b}^2 - 3\bar{a}\bar{c} \geq 0$, which can be proved by contradiction. In fact, if $\bar{b}^2 - 3\bar{a}\bar{c} < 0$ then the function K has no real roots and therefore the function L is monotonically increasing or monotonically decreasing. Therefore L cannot have three distinct roots, which is a contradiction with the fact that $\Delta > 0$. Note that the function R must have at least one inflection point since $\bar{b}^2 - 3\bar{a}\bar{c} \geq 0$. An example is shown in Fig. 5d.

It is clear that for the first three cases the peak value of $R(t_f)$ is at one of the boundary instants, i.e., $max(R(t)) = max(R(0), R(t_f))$. Since the boundary conditions are required

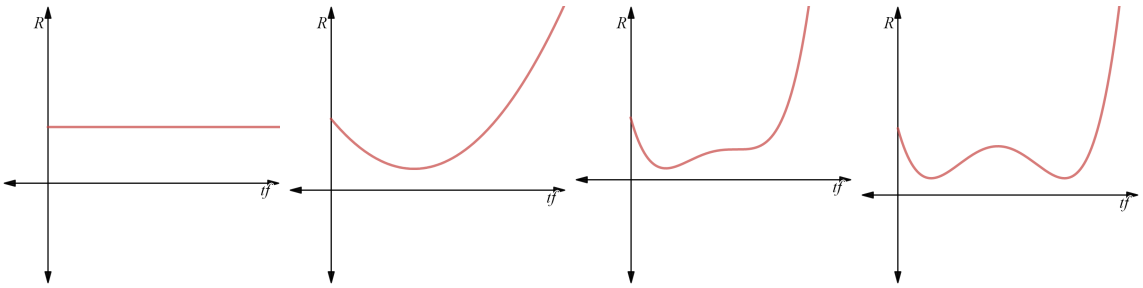

(a) $R(t_f)$ for case 1 (b) $R(t_f)$ for case 2 (c) $R(t_f)$ for case 3 (d) $R(t_f)$ for case 4

Figure 5: Possible cases for the shape of function $R(t_f)$

to be feasible, the maximum velocity constraint is naturally verified when the peak value is located at a boundary point. For the case 4) we can find the root t_m of function $L(t)$ between two inflection points of L, namely t_1, t_2 (which are the same point if $\bar{b}^2 - 3\bar{a}\bar{c} = 0$). The pseudocode is as follows:

Algorithm 3 finding the maximum speed

$maxV = \sqrt{max(R(0), R(t_f))}$;
if $\bar{a} \neq 0$ & $\Delta > 0$ **then**
  $t_1 = \frac{-\bar{b}-\sqrt{\bar{b}^2-3\bar{a}\bar{c}}}{3\bar{a}}, t_2 = \frac{-\bar{b}+\sqrt{\bar{b}^2-3\bar{a}\bar{c}}}{3\bar{a}}$;
  $t_m = (t_1 + t_2)/2$;
  $t_m = NR(K, t_m)$;
  if $t_m < t_f$ **then**
    $maxV = \sqrt{max(R(t_m), R(0), R(t_f))}$;
  end if
end if

where $NR(R, t_m)$ is the routine for the Newton-Raphson method defined previously. After obtaining the maximum velocity for a given flight time, we propose using the Bisection Search Method to find the shortest flight time, such that the maximum velocity for that flight is below the limit. The termination error will be assumed to be $0.1s$, which is small enough to work well in most practical applications. The pseudocode is as follows for a given t_f:

Algorithm 4 finding the optimal flight time satisfying the velocity constraint

while $maxV(t_f) > V_{max}$ **do**
  $t_f = 2t_f$;
end while
$t_{f_0} = t_f/2$;
while $|t_f - t_{f_0}| > 0.1$ **do**
  $t_{f_1} = (t_f + t_{f_0})/2$;
  if $maxV(t_{f_1}) > V_{max}$ **then**
    $t_{f_0} = t_{f_1}$;
  else
    $t_f = t_{f_1}$;
  end if
end while

2.3 Simulation Results

Assume that for the initial state $x_0 = [0, 0, 1, 1, 0, 0]^T$ the aircraft receives a command to go to the destination $x_f = [10, 2, 5, 0, 0, 0]^T$ at a time $t_f = 5s$. We consider $C_I = 0.1, g = 9.8m/s^2$. The parameters for this simulation are collected in Table 2.

Table 2: Simulation parameters

Parameter	Value
p_0 (m)	0,0,1
v_0 (m/s)	1,0,0
p_f (m)	10,2,5
v_f (m/s)	0,0,0
C_I	0.1
g (m/s^2)	9.8
V_{max} (m/s)	20

The optimal cost as a function of flight time is shown in Fig. 6. It is clear that there is an optimal time minimizing the total cost, which is not equal to $5s$. The optimal time calculated with Newton-Raphson Method is $2.4977s$ after only 7 iterations. The result is consistent with the exact solution of (25). Fig. 7a shows the 3D trajectory for $t_f = 5s$. Fig. 7b shows the optimal trajectory for the optimal flight time. The plots of 3D trajectory, velocity, and acceleration are also shown. Black dotted lines are magnitude values.

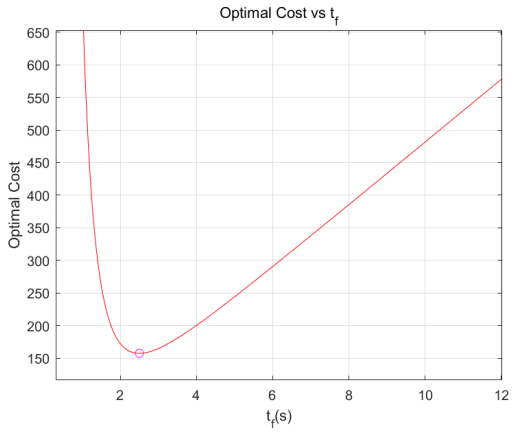

Figure 6: Optimal cost for different t_f.

2.3.1 Discussion

The optimal flight time is close to half of $5s$. The peak acceleration for the optimal flight time is approximately 5 times higher than for the solution with a flight time of $5s$. The effects of C_I on the total cost, optimal flight time, and peak velocity are shown in Fig. 8 and Fig. 9 for another set of boundary conditions for the generality $x_0 = [-0.5, -1.9, 1, 1.6, 3.7, 1]^T, x_f = [10, 2, 5, -0.3, 0.7, 0]^T$. A higher value of C_I leads to a shorter flight time, and higher peak velocity as shown in Fig. 9. Please note that the results of Fig. 8 do not mean that a higher C_I value should be avoided because of the higher total cost incurred. It simply presents the situation when flight time has a higher weight in the total cost.

2.3.2 Optimal passenger satisfaction trajectory

For the same two-point boundary value constraints, the optimal passenger satisfaction trajectory is generated. Only 9 iterations were needed to find the optimal $t_f = 10.3206s$, which is also consistent with the exact solution. An interesting fact is that the optimal flight time is longer than the previous case with the same boundary conditions because the gravity is excluded for this case, which implies a lower time-related cost for the same value of C_I. The optimal trajectory is shown in Fig. 10. The effects of t_f and C_I on the total cost give similar results to the case seen previously and are therefore not repeated here.

2.3.3 Optimal trajectory verifying peak velocity constraint

Continuing with the previous scenario, suppose that at the initial state $x_0 = [0, 0, 1, 3, -1, 2]^T$, the aircraft receives a command to arrive at the destination $x_f = [3150, 2713, 57, 0, 0, 0]^T$ at

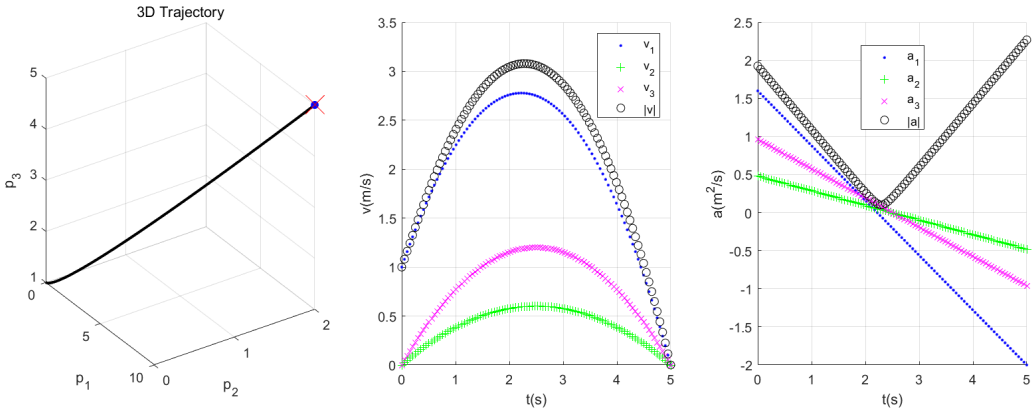

(a) Optimal trajectory, velocity and acceleration for t_f=5s.

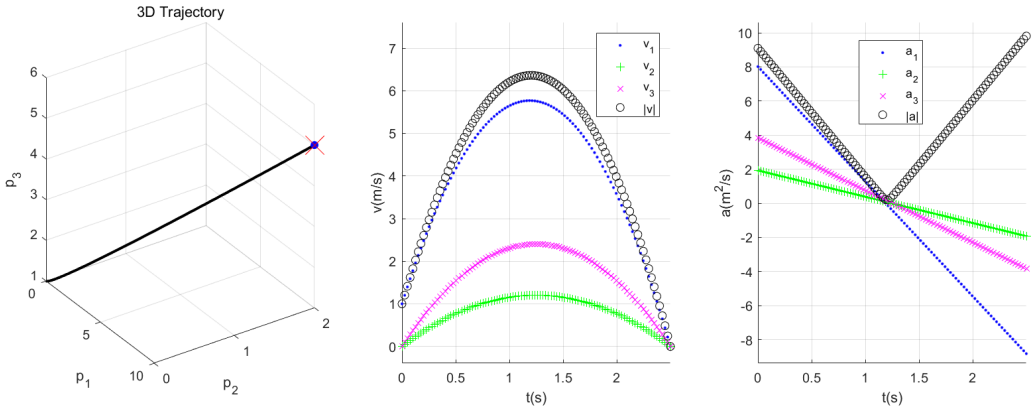

(b) Optimal trajectory, velocity and acceleration for t_f=2.4977s.

Figure 7: Optimal trajectories for two t_f values.

a flight time of $t_f = 250s$. Note that this flight time might not be feasible because there is a peak velocity constraint of $V_{max} = 20m/s$. In fact, the maximum velocity during the optimal flight trajectory for $t_f = 250s$ is $24.5546m/s$. Using our algorithm, the optimal flight time for which the trajectories respect the peak velocity limit is $t_f^* = 305.9440s$, which is comparable with $305.9209s$ obtained from the Golden Section Search & Successive Parabolic Interpolation Method(GSSSPIM) [76] with the same termination tolerance. However, the computational time of our algorithm is less than one quarter of the time taken by GSSSPIM ($1.961642s$ vs $9.180235s$) with the same computer and running environment. The trajectory is shown in Fig. 11. Clearly, the velocity verifies the constraint and the two-point boundary conditions are met. The acceleration is less than $0.3m/s^2$ for the whole flight.

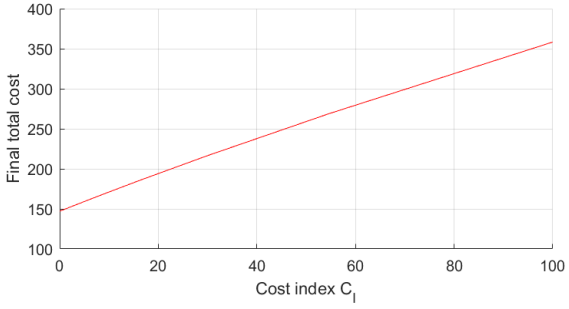

Figure 8: Effect of C_I on total cost.

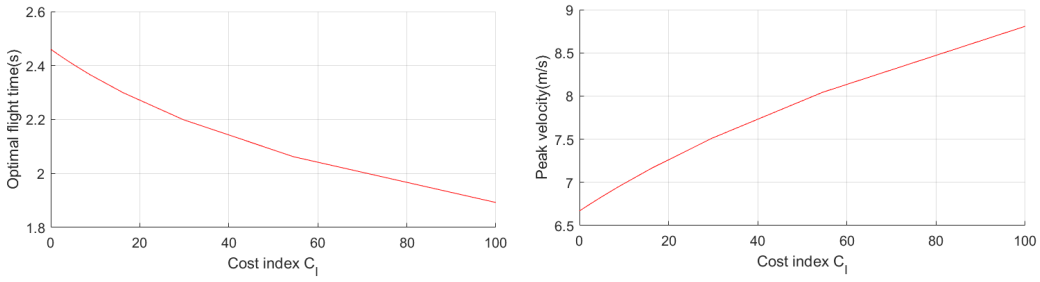

(a) Effect of C_I on optimal flight time.

(b) Effect of C_I on peak velocity.

Figure 9: Effects of C_I on optimal parameters.

2.4 Conclusions

This chapter formulated and solved an optimal trajectory generation problem for minimizing damage in package delivery. The same methodology could be used for maximizing passenger comfort during flight with only minor modifications. An analytical solution in 3D space was obtained for arbitrary feasible boundary conditions. The proposed methodology can generate the optimal flight trajectory for a given flight time. Additionally, an optimal time can be determined. Furthermore, the methodology was extended to provide solutions that satisfy a peak velocity constraint. The effects of a parameter called the cost index on the optimal solution were also discussed.

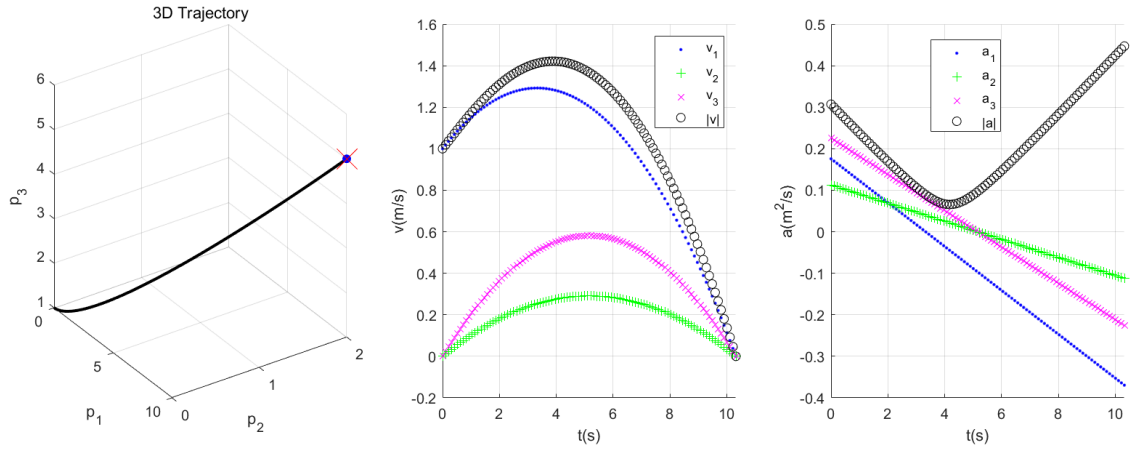

Figure 10: Optimal passenger satisfaction trajectory, velocity and acceleration for optimal t_f.

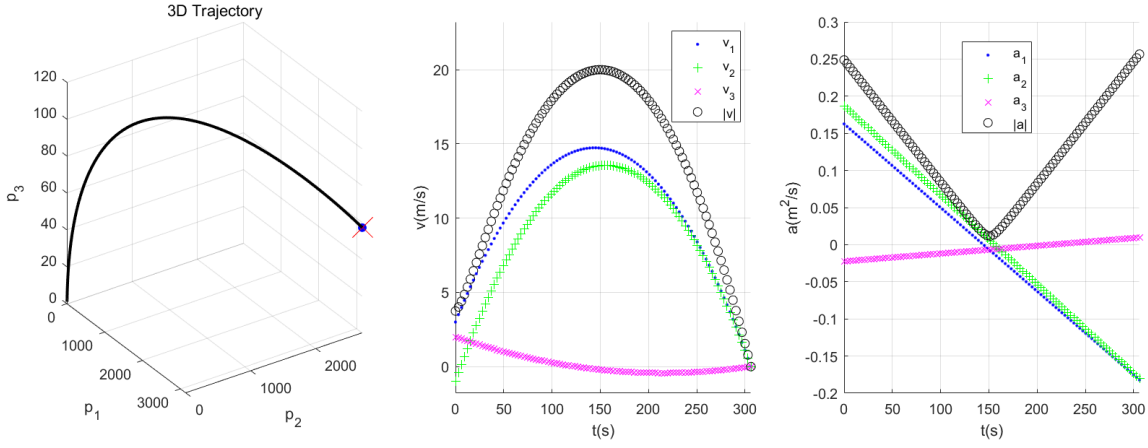

Figure 11: Optimal trajectory, velocity and acceleration satisfying maximal velocity limit.

Chapter 3

Optimal Trajectory Trading-off Control Effort and Flight Time for Hovering Vehicles

3.1 Introduction

After viewing the optimal trajectory from the passenger's point of view, we look at the problem from the operator's side in this chapter. The flight trajectory for hovering vehicles which optimizes a combination of control effort and flight time will be presented.

In the first half, we present the trajectory neglecting wind. Compared to the previous work in the literature, the main contributions of this part are as follows:

- the proposed approach can find the analytical solution for either a fixed time or a free time. Additionally, for long haul flights, an approximate solution is presented to reduce the computational time. A characteristic parameter is proposed to decide whether to use the analytical solution or the approximation,
- the approach is extended to satisfy peak velocity constraints.

In the second half, we present the optimal trajectory in a constant wind shear field. Compared to the previous work in the literature, the main contributions of this section are as follows:

- an analytical solution is obtained to trade-off control effort and flight time for hovering vehicles in a constant wind shear field for arbitrary boundary conditions,
- the proposed approach accommodates both fixed and free flight times and satisfies peak thrust constraints.

The structure of this chapter is as follows. Section 3.2 presents the problem formulation and the detailed solution of the optimal trajectory generation problem, including the optimal trajectory and the optimal flight time. Simulation results are presented in section 3.3. Next, in section 3.4, the modified problem formulation considering wind is presented, while the detailed solution of the optimal trajectory appears in section 3.5. Simulation results are presented in section 3.6. Concluding remarks are stated in section 3.7.

3.2 Optimal Trajectory without Wind

3.2.1 Problem Description

Assume that an aircraft at current state x_0 receives a command to reach the destination x_f at time t_f. The problem to be solved in this chapter is to generate the trajectory between x_0 and x_f that optimizes a functional that trades off control effort and flight time. This optimal trajectory is to be found for both a fixed and a free flight time.

To formulate and solve this problem we make the following assumptions:

1. The vehicle conserves its mass, or mass depletion is sufficiently slow. Electric vehicles naturally fall into this condition.

2. The only forces acting on the aircraft are thrust, drag and weight.

3. The wind effect and air density variation are ignored.

4. The drag is linear in the velocity written as

$$D = -k_d v \tag{39}$$

   where D is drag, v is velocity, and k_d is assumed to be a constant for a given flight. For lower Reynold's numbers ($Re < 10^3$), this is a reasonable assumption called linear Stokes drag [77, 77]. For higher Reynold's numbers, it is just an approximation and valid only within a small range in the neighborhood of the target velocity.

3.2.2 Problem Formulation

Define the state vector $x = [p_1, p_2, p_3, v_1, v_2, v_3]^T$, where p is the vector of position coordinates, v is the vector of velocity coordinates. The system dynamics are

$$\begin{bmatrix} \dot{p_1} \\ \dot{p_2} \\ \dot{p_3} \\ \dot{v_1} \\ \dot{v_2} \\ \dot{v_3} \end{bmatrix} = \begin{bmatrix} 0 & 0 & 0 & 1 & 0 & 0 \\ 0 & 0 & 0 & 0 & 1 & 0 \\ 0 & 0 & 0 & 0 & 0 & 1 \\ 0 & 0 & 0 & 0 & 0 & 0 \\ 0 & 0 & 0 & 0 & 0 & 0 \\ 0 & 0 & 0 & 0 & 0 & 0 \end{bmatrix} \begin{bmatrix} p_1 \\ p_2 \\ p_3 \\ v_1 \\ v_2 \\ v_3 \end{bmatrix} + \begin{bmatrix} 0 & 0 & 0 \\ 0 & 0 & 0 \\ 0 & 0 & 0 \\ 1 & 0 & 0 \\ 0 & 1 & 0 \\ 0 & 0 & 1 \end{bmatrix} \begin{bmatrix} a_1 \\ a_2 \\ a_3 \end{bmatrix} \tag{40}$$

$$\begin{bmatrix} T_1 \\ T_2 \\ T_3 \end{bmatrix} = m \left(\begin{bmatrix} a_1 \\ a_2 \\ a_3 \end{bmatrix} + \begin{bmatrix} 0 \\ 0 \\ g \end{bmatrix} \right) + k_d \begin{bmatrix} v_1 \\ v_2 \\ v_3 \end{bmatrix} \tag{41}$$

The optimal control problem is

$$\begin{aligned} J = \min_{T} \quad & \int_0^{t_f} \frac{1}{2} T^T T + C_I dt \\ s.t. \quad & (40), (41) \\ & x(t_0) = x_0 \\ & x_f \text{ given} \end{aligned} \tag{42}$$

where C_I is the ratio of cost of time and cost of control effort. Define

$$\lambda = \frac{\partial J(x)}{\partial x} \tag{43}$$

$$H = L(T) + \lambda^T f(x, T) \tag{44}$$

where $L(T) = \frac{1}{2} T^T T + C_I$ and $f(x, T)$ is defined in (40)-(41). Following the same procedure in section 2.2, one needs the necessary conditions below for a minimizer

$$\frac{\partial H^*}{\partial T} = 0 \tag{45}$$

$$\frac{\partial H^*}{\partial x} = -\dot{\lambda} \tag{46}$$

3.2.3 Optimal trajectory solution

Theorem 3.2.1 *The optimal flight trajectory, which is the solution to problem* (42) *is*

$$\begin{bmatrix} p_1 \\ p_2 \\ p_3 \end{bmatrix} = \begin{bmatrix} -\frac{C_1}{k_d^2} t - \frac{C_4}{2k_d^2} e^{\frac{k_d}{m} t} - \frac{C_7 m}{k_d} e^{-\frac{k_d}{m} t} + C_{10} \\ -\frac{C_2}{k_d^2} t - \frac{C_5}{2k_d^2} e^{\frac{k_d}{m} t} - \frac{C_8 m}{k_d} e^{-\frac{k_d}{m} t} + C_{11} \\ -\frac{C_3}{k_d^2} t - \frac{C_6}{2k_d^2} e^{\frac{k_d}{m} t} - \frac{C_9 m}{k_d} e^{-\frac{k_d}{m} t} + C_{12} \end{bmatrix} \tag{47}$$

where p_i is the position, k_d is the drag coefficient, m is the mass, and

$$\begin{bmatrix} C_i \\ C_{i+3} \\ C_{i+6} \\ C_{i+9} \end{bmatrix} = \begin{bmatrix} -v_{0i}k_d^2 - \frac{k_d}{2m}C_{i+3} + C_{i+6}k_d^2 \\ \frac{(p_{fi}-p_{0i})+(v_{fi}-v_{0i})\frac{m}{k_d}-v_{0i}t_f-\frac{(v_{fi}-v_{0i})t_f e^{\frac{k_d}{m}t_f}}{e^{\frac{k_d}{m}t_f-1}}}{\frac{t_f}{2mk_d}\left(e^{\frac{k_d}{m}t_f+1}\right)-\frac{1}{k_d^2}\left(e^{\frac{k_d}{m}t_f-1}\right)} \\ -\frac{(v_{fi}-v_{0i})e^{\frac{k_d}{m}t_f}}{e^{\frac{k_d}{m}t_f-1}} - \frac{e^{\frac{k_d}{m}t_f}}{2mk_d}C_{i+3} \\ p_{0i} + \frac{1}{2k_d^2}C_{i+3} + \frac{m}{k_d}C_{i+6} \end{bmatrix} \tag{48}$$

for $i = 1, 2, 3$.

Proof: The Hamiltonian of (42) is

$$\begin{aligned} H &= \frac{1}{2}T^2 + \lambda_1\dot{p_1} + \lambda_2\dot{p_2} + \lambda_3\dot{p_3} + \lambda_4\dot{v_1} + \lambda_5\dot{v_2} + \lambda_6\dot{v_3} + C_I \\ &= \frac{1}{2}(T_1^2 + T_2^2 + T_3^2) + \lambda_1 v_1 + \lambda_2 v_2 + \lambda_3 v_3 + C_I + \\ &\frac{\lambda_4}{m}(T_1 - k_d v_1) + \frac{\lambda_5}{m}(T_2 - k_d v_2) + \frac{\lambda_6}{m}(T_3 - k_d v_3 - mg) \end{aligned} \tag{49}$$

From (45),

$$\frac{\partial H^*}{\partial T} = \begin{bmatrix} T_1 \\ T_2 \\ T_3 \end{bmatrix} + \frac{1}{m}\begin{bmatrix} \lambda_4 \\ \lambda_5 \\ \lambda_6 \end{bmatrix} = \begin{bmatrix} 0 \\ 0 \\ 0 \end{bmatrix} \tag{50}$$

$$T^* = \frac{1}{m}[-\lambda_4, -\lambda_5, -\lambda_6]^T \tag{51}$$

$$H^* = -\frac{1}{2m^2}(\lambda_4^2 + \lambda_5^2 + \lambda_6^2) + \lambda_1 v_1 + \lambda_2 v_2 + \lambda_3 v_3 - \frac{k_d}{m}(\lambda_4 v_1 + \lambda_5 v_2 + \lambda_6 v_3) - \lambda_6 g + C_I \tag{52}$$

From (46),

$$\frac{\partial H^*}{\partial p} = \begin{bmatrix} 0 \\ 0 \\ 0 \end{bmatrix} = \begin{bmatrix} -\dot{\lambda}_1 \\ -\dot{\lambda}_2 \\ -\dot{\lambda}_3 \end{bmatrix}, \frac{\partial H^*}{\partial v} = \begin{bmatrix} \lambda_1 - \frac{k_d}{m}\lambda_4 \\ \lambda_2 - \frac{k_d}{m}\lambda_5 \\ \lambda_3 - \frac{k_d}{m}\lambda_6 \end{bmatrix} = \begin{bmatrix} -\dot{\lambda}_4 \\ -\dot{\lambda}_5 \\ -\dot{\lambda}_6 \end{bmatrix} \tag{53}$$

$$[\lambda_1, \lambda_2, \lambda_3]^T = [C_1, C_2, \bar{C}_3]^T \tag{54}$$

$$\begin{bmatrix} \lambda_4 \\ \lambda_5 \\ \lambda_6 \end{bmatrix} = \begin{bmatrix} \frac{C_1 m}{k_d} + C_4 e^{\frac{k_d}{m}t} \\ \frac{C_2 m}{k_d} + C_5 e^{\frac{k_d}{m}t} \\ \frac{\bar{C}_3 m}{k_d} + C_6 e^{\frac{k_d}{m}t} \end{bmatrix} = -m\begin{bmatrix} T_1 \\ T_2 \\ T_3 \end{bmatrix} \tag{55}$$

From (41),

$$\dot{v} = a = \frac{1}{m}\begin{bmatrix} -\frac{C_1}{k_d} - \frac{C_4}{m}e^{\frac{k_d}{m}t} - k_d v_1 \\ -\frac{C_2}{k_d} - \frac{C_5}{m}e^{\frac{k_d}{m}t} - k_d v_2 \\ -\frac{\bar{C}_3}{k_d} - \frac{C_6}{m}e^{\frac{k_d}{m}t} - k_d v_3 - mg \end{bmatrix} \tag{56}$$

Define C_3 as

$$C_3 = \bar{C}_3 + mgk_d \tag{57}$$

Integrating (56) and using (57) yields

$$v = \begin{bmatrix} -\frac{C_1}{k_d^2} - \frac{C_4}{2mk_d} e^{\frac{k_d}{m}t} + C_7 e^{-\frac{k_d}{m}t} \\ -\frac{C_2}{k_d^2} - \frac{C_5}{2mk_d} e^{\frac{k_d}{m}t} + C_8 e^{-\frac{k_d}{m}t} \\ -\frac{C_3}{k_d^2} - \frac{C_6}{2mk_d} e^{\frac{k_d}{m}t} + C_9 e^{-\frac{k_d}{m}t} \end{bmatrix} \tag{58}$$

Integrating (58), (47) is obtained.
The boundary conditions are

$$\begin{bmatrix} p(0) \\ v(0) \end{bmatrix} = x_0, \begin{bmatrix} p(t_f) \\ v(t_f) \end{bmatrix} = x_f \tag{59}$$

After solving (59) using (47), (58), we get (48). We observe that the denominator of C_{i+3} will never be zero. To show this, let $Q = \frac{k_d t_f}{m} > 0$, then the denominator equal to zero is equivalent to $Q(e^Q + 1) - 2(e^Q - 1) = 0$. Since the derivative of the left-hand-side is $(Q-1)e^Q+1$. It is monotonically increasing, and when $Q = 0$, $(Q-1)e^Q+1 = 0$. Therefore, $Q(e^Q + 1) - 2(e^Q - 1) > 0(e^0 + 1) - 2(e^0 - 1) = 0$. Q.E.D.

Theorem 3.2.2 *The optimal cost for a given flight time t_f is*

$$\begin{aligned} J^* = \left(\frac{1}{2}m^2g^2 + C_I\right) t_f - mg\left[\frac{C_3}{k_d}t_f + \frac{C_6}{k_d}\left(E(t_f) - 1\right)\right] + \\ \sum_{i=1}^{3}\left[\frac{C_i^2}{2k_d^2}t_f + \frac{C_{i+3}^2}{4k_d m}\left(E(2t_f) - 1\right) + \frac{C_i C_{i+3}}{k_d^2}\left(E(t_f) - 1\right)\right] \end{aligned} \tag{60}$$

where $E(t) = e^{\frac{k_d}{m}t}$.

Proof: From (55), (57), we get

$$\begin{bmatrix} T_1 \\ T_2 \\ T_3 \end{bmatrix} = \begin{bmatrix} -\frac{C_1}{k_d} - \frac{C_4}{m}E(t) \\ -\frac{C_2}{k_d} - \frac{C_5}{m}E(t) \\ -\frac{C_3}{k_d} - \frac{C_6}{m}E(t) + mg \end{bmatrix} \tag{61}$$

By plugging (61) into the cost function in (42) and integrating, expression (60) is obtained. Q.E.D.

Approximation 1: For longer t_f, i.e. $\frac{k_d}{m}t_f > 5$, an approximate solution is

$$p_i = p_{0i} + (v_{fi} + \frac{k_d}{m}l_{f_i})t - l_{f_i}E(t - t_f) + \left[\frac{m}{k_d}(v_{fi} - v_{0i}) + l_{f_i}\right]\left(E(-t) - 1\right) \tag{62}$$

where $i = 1, 2, 3$, and

$$l_f = \frac{(p_f - p_0) + \frac{(v_f - v_0)}{k_d} m - v_f t_f}{\frac{k_d}{m} t_f - 2} = -\frac{m v_f}{k_d} + \frac{(p_f - p_0) - \frac{m}{k_d}(v_f + v_0)}{\frac{k_d}{m} t_f - 2} \tag{63}$$

$$\begin{aligned} J^* = &\left(\frac{1}{2} m^2 g^2 + C_I + m g k_d v_{f3} + g k_d^2 l_{f_3} \right) t_f - 2 m g k_d l_{f_3} + \sum_{i=1}^{3} \left[\frac{k_d^2}{2} t_f \left(v_{fi} + \frac{k_d}{m} l_{f_i} \right)^2 \right. \\ &\left. + \frac{k_d^3}{m} l_{f_i}^2 - 2 k_d^2 l_{f_i} \left(v_{fi} + \frac{k_d}{m} l_{f_i} \right) \right] \end{aligned} \tag{64}$$

In fact, when $\frac{k_d}{m} t_f > 5$, the following hold

$$E(t_f) > 100 \gg 1 \tag{65}$$

$$E(t_f) \pm 1 \approx E(t_f) \tag{66}$$

One can then approximate C_{i+3}, for $i = 1, 2, 3$, as

$$C_{i+3} = \frac{(p_{fi} - p_{0i}) + (v_{fi} - v_{0i}) \frac{m}{k_d} - v_{fi} t_f}{\left(\frac{t_f}{2 m k_d} - \frac{1}{k_d^2} \right) E(t_f)} = \frac{2 k_d^2}{E(t_f)} l_{f_i} \tag{67}$$

Then (48) becomes

$$\begin{bmatrix} C_i \\ C_{i+3} \\ C_{i+6} \\ C_{i+9} \end{bmatrix} = \begin{bmatrix} -k_d^2 (v_{fi} + \frac{k_d}{m} l_{f_i}) \\ \frac{2 k_d^2}{E(t_f)} l_{f_i} \\ -(v_{fi} - v_{0i}) - \frac{k_d}{m} l_{f_i} \\ p_{0i} - \frac{m}{k_d}(v_{fi} - v_{0i}) - l_{f_i} \end{bmatrix} \tag{68}$$

Using (68) in (47) yields (62). Plugging (68) into (60), (64) is obtained. Accordingly, the new velocity profile is

$$v_i = (v_{fi} + \frac{k_d}{m} l_{f_i}) - \frac{k_d}{m} l_{f_i} E(t - t_f) - \left[(v_{fi} - v_{0i}) + \frac{k_d}{m} l_{f_i} \right] E(-t) \tag{69}$$

Remark 3.2.3 *$E(t_f)$ and l_f are a scalar and a vector, respectively, for a given set of boundary conditions and flight time t_f.*

Remark 3.2.4 *The condition for the approximation can be loosened to $\frac{k_d}{m} t_f > 3$, so as to obtain an approximation error $\frac{E(t_f)}{E(t_f)-1} \approx 1.0524$, meaning about 5% of relative error for this approximation when $\frac{k_d}{m} t_f = 3$. The approximate trajectory will be shown in the next section. When $\frac{k_d}{m} t_f < 3$, Theorem 3.2.1 and 3.2.2 have to be applied. The optimal flight time t_f is sought with numerical methods for 1D optimization problems, such as Golden Section Search, or Successive Parabolic Interpolation [76], because there are over 20 terms in the cost function, which makes the gradient based optimization too expensive to analyze and solve.*

We define the characteristic parameter

$$CV = \frac{3C_D}{4}\frac{\rho_{air}}{\rho_{craft}}\frac{dist}{l} \tag{70}$$

where C_D is the drag coefficient, ρ_{air}, ρ_{craft} is air density and effective aircraft density, respectively, $dist$ is the flight distance, and l is the aircraft length. This parameter determines whether to use the theoretical solution ($CV < 3$) or the approximation ($CV \geq 3$).

Considering the smallest outer sphere surrounding the hovering aircraft, the diameter of the sphere equals to the aircraft length l. The volume of the sphere is $\frac{1}{6}\pi l^3 = \frac{2}{3}Al$, where A is the effective area of the outer sphere surrounding the aircraft defined as $A = \frac{1}{4}\pi l^2$. Define the effective aircraft density ρ_{craft} as mass divided by the volume of the sphere. Choosing k_d with average velocity magnitude v_{avg}, we expand the terms as

$$\frac{k_d}{m}t_f = \frac{\frac{1}{2}C_D\rho_{air}Av_{avg}t_f}{\rho_{craft}A\frac{2}{3}l} = \frac{3C_D}{4}\frac{\rho_{air}}{\rho_{craft}}\frac{dist}{l} \tag{71}$$

Note that C_D is a function of the Reynold's number, which is defined as

$$Re = \frac{\rho_{air}}{\mu}v_{avg}l \tag{72}$$

For a given aircraft, $\frac{k_d}{m}t_f$ is a function of the flying environment (atmosphere), estimated average speed, and flight distance. Therefore, it can be regarded as a characteristic parameter for the flight trajectory.

Theorem 3.2.5 *There is at most one peak velocity during flight.*

Proof: R is the square of the velocity magnitude, and can be obtained from (58) as

$$\begin{aligned} R &= |v(t)|^2 \\ &= \sum_{i=1}^{3}\left[\frac{C_i^2}{k_d^4} + \frac{C_{i+3}^2}{4m^2k_d^2}E(2t) + C_{i+6}^2E(-2t) + \frac{C_iC_{i+3}}{mk_d^3}E(t) - \frac{2C_iC_{i+6}}{k_d^2}E(-t) - \frac{C_{i+3}C_{i+6}}{mk_d}\right] \end{aligned} \tag{73}$$

Define

$$
\begin{aligned}
a &= \sum_{i=1}^{3} \frac{C_{i+3}^2}{4m^2k_d^2} \geq 0 \\
b &= \sum_{i=1}^{3} C_{i+6}^2 \geq 0 \\
c &= \sum_{i=1}^{3} \frac{C_i C_{i+3}}{mk_d^3} \\
d &= \sum_{i=1}^{3} -\frac{2C_i C_{i+6}}{k_d^2} \\
e &= \sum_{i=1}^{3} \frac{C_i^2}{k_d^4} - \frac{C_{i+3}C_{i+6}}{mk_d}
\end{aligned}
\tag{74}
$$

Then we have

$$
\begin{aligned}
R &= aW^2 + \frac{b}{W^2} + cW + \frac{d}{W} + e \\
W &= E(t) \in [1, E(t_f)]
\end{aligned}
\tag{75}
$$

The function R is differentiable on t since it is the summation of differentiable functions. Additionally, W is monotonic on t without sign change, and is never zero. Define the function Q as

$$
Q = \frac{\partial R}{\partial W} W^3 = (2aW - \frac{2b}{W^3} + c - \frac{d}{W^2})W^3 = \left(2aW^4 + cW^3 - dW - 2b\right) \tag{76}
$$

Let W_m be the zero-crossing point of the function Q from positive to negative values within the interval $W \in [1, E(t_f)]$, which corresponds to the maximizer of the function R. Therefore, the peak value of R during the flight is found as

$$
max(R) = max\left(R(1), R(E(t_f)), R(W_m)\right) \tag{77}
$$

The following two cases are possible:

1. $a = 0$.

   Then we have $C_{i+3} = 0, i \in \{1, 2, 3\}$, so that $c = 0$, and then $Q = -dW - 2b$. Since $-2b \leq 0$, there is no zero-crossing point of function Q from positive to negative values within the interval $W \in [1, E(t_f)]$. An example is shown in Fig. 12a. The single peak velocity will therefore occur at either $W = 1$ or $W = E(t_f)$.

2. $a \neq 0$.

   The function Q is a quartic function. Only when Q has four distinct real roots, there are two zero-crossing points in the direction from positive to negative values. An example is shown in Fig. 12d. Otherwise, there is at most one zero-crossing point

from positive to negative values, for example in Fig. 12b and Fig. 12c. Assume there are two maximizers in $W > 0$. Note that we must have $Q(0) > 0$ because Q decreases on the left of the first root. Since $Q(W = 0) = -2b \leq 0$, we obtain a contradiction. Therefore, there must be at most one maximizer in $W > 0$. Q.E.D.

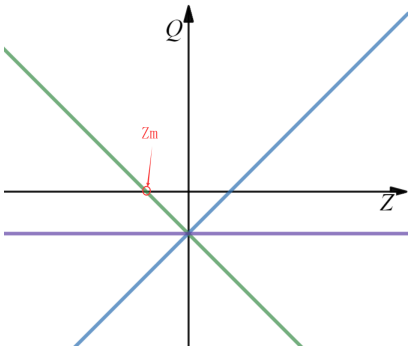

(a) Function Q for case 1

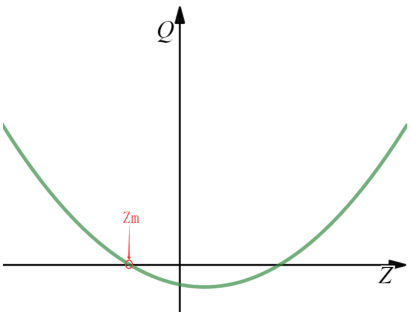

(b) Function Q for case 2, two simple roots

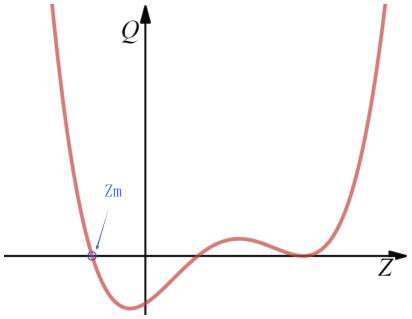

(c) Function Q for case 3, two simple roots and one double root

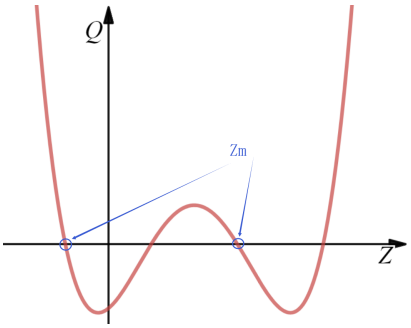

(d) Function Q for case 4, four distinct roots

Figure 12: Curves of function R for all cases

Remark 3.2.6 *A proposed solution to find the feasible flight time t_f which verifies the peak velocity constraint is to find the shortest time such that $max(R) \leq V_{max}^2$.*

3.3 Simulation Results

Two cases are studied in this section, one being a smaller electric rotorcraft, the other being a bigger manned electric helicopter. Their k_d is calculated with a coefficient of drag C_D chosen from reference [77] assuming that they are rough spherical objects and with v_{avg} obtained by dividing distance with time. In Fig. 15, the dotted line is the trajectory from Theorem 3.2.1, while the crossed line is the approximate solution from Approximation 1.

3.3.1 Case 1: Smaller rotorcraft

Let $x_0 = [-1.5, 0, 1, 1, 0, -1]^T$ and $x_f = [10, 2, 5, 0, 2, 0]^T$. Taking the DJI Phantom 4 Pro [78] as an example, $m = 1.388kg, l = 0.35m, C_D = 0.3, C_I = 10$. The air density $\rho_{air} = 1.225kg/m^3$ is chosen from reference [4] at sea level. The parameters for this simulation are collected in Table 3. The parameter $CV = 0.15716 \ll 3$. In this case, Theorem 3.2.1

Table 3: Simulation parameters

Parameter	Value
$p_0\ (m)$	-1.5,0,1
$v_0\ (m/s)$	1,0,-1
$p_f\ (m)$	10,2,5
$v_f\ (m/s)$	0,2,0
C_I	10
$m\ (kg)$	1.388
$l\ (m)$	0.35
C_D	0.3
$\rho_{air}\ (kg/m^3)$	1.225
$g\ (m/s^2)$	9.8
$V_{max}\ (m/s)$	20

and 3.2.2 have to be used. The optimal flight time is $t_f = 2.6813s$. Fig. 13 shows the optimal 3D trajectory and the corresponding velocity, acceleration, thrust, position and cost over time. The final position error is $1.819e^{-12}m$, i.e., it is a factor of $1.4742e^{-13}$ of the whole distance of $12.3390m$, merely because of roundoff error. The velocity stays well within range under the upper limit of $20m/s$. The velocity peak and valley of acceleration in the middle are caused by the relatively low boundary velocities. The thrust takes values between $13 \sim 23N$. The final cost is 355.8. The Pareto trade-off curve of this flight is depicted in Fig. 14, which illustrates the tradeoff between the flight time and control effort, and indicates that a larger C_I leads to a shorter flight time and higher control effort.

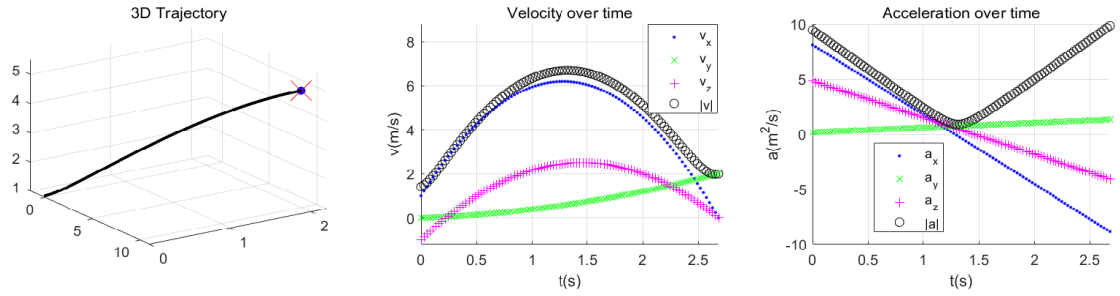

Figure 13: Optimal trajectory for smaller rotorcraft.

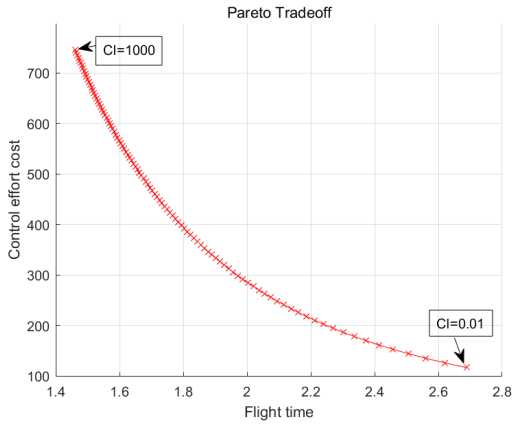

Figure 14: Pareto trade-off of C_I

3.3.2 Case 2: Larger manned helicopter

Let $x_0 = [-1.5, 0, 10, 30, 5, 3]^T$ and $x_f = [17810, 26370, 3645, 4, 32, 0]^T$. Taking the Sikorsky Firefly [79] as an example, $m = 930kg, l = 2.54m, C_D = 0.3, C_I = 10$. The air density $\rho_{air} = 1.0251kg/m^3$ is chosen from reference [79] at the middle altitude of the two boundary points. The parameters of this simulation are collected in Table 4. The parameter

Table 4: Simulation parameters

Parameter	Value
$p_0\ (m)$	-1.5,0,10
$v_0\ (m/s)$	30,5,3
$p_f\ (m)$	17810,26370,3645
$v_f\ (m/s)$	4,32,0
C_I	10
$m\ (kg)$	930
$l\ (m)$	2.54
C_D	0.3
$\rho_{air}\ (kg/m^3)$	1.0251
$g\ (m/s^2)$	9.8
$V_{max}\ (m/s)$	45

$CV = 26.8335 > 3$, so either Approximation 1 or Theorem 3.2.5 can be used. The optimal flight time is $t_f = 736.3338s$. Fig. 15 shows the optimal 3D trajectory and the corresponding velocity, acceleration, thrust, position and cost over time. The lines of the exact solution and the approximate one match well with each other, meaning that the approximate solution can represent the exact solution with minor errors. The calculation is much faster for the approximate solution. The final position error is $1.99e^{-09}m$, i.e., it is a factor of $6.2269e^{-14}$ of the whole distance of $32028.73m$. The acceleration plot shows that the trajectory has a

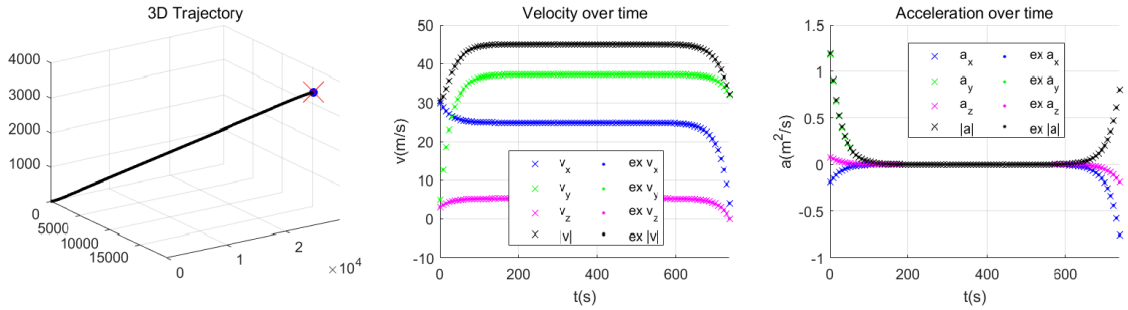

Figure 15: Optimal trajectory for manned helicopter.

peak value of less than $1.5m/s^2$. The thrust magnitude is slowly varying and the cost is approximately linear as a function of time. For this long haul example, a cruise-like phase appears during the flight.

3.4 Optimal Trajectory in Constant Wind Shear Field

3.4.1 Problem description

In this section, we present the optimal trajectory in constant wind shear field. Compared to section 3.2, the assumptions become:

1. The vehicle conserves its mass, or mass depletion is sufficiently slow. Electric vehicles naturally fall into this situation.

2. The only forces acting on the aircraft are thrust, drag and gravity, which is the case for rotorcraft hovering vehicles.

3. There is a constant wind shear field

$$\mathbf{v}_a = \mathbf{v}_{a_0} + \mathbf{w}_0^T(\mathbf{p} - \mathbf{p}_0)\frac{\mathbf{v}_{a_0}}{|\mathbf{v}_{a_0}|} \tag{78}$$

   where $\mathbf{v}_a$ is the wind velocity, $\mathbf{v}_{a_0}$ is the nonzero wind velocity at the initial state, $\mathbf{w}_0$ is the shear vector, which is the gradient vector of the wind speed, $\mathbf{p}$ is the vector of position coordinates, $\mathbf{p}_0$ is the initial position.

4. The drag is linear, written as

$$\mathbf{D} = -k_d(\mathbf{v} - \mathbf{v}_a) \tag{79}$$

   where $\mathbf{v}$ is the ground speed, and k_d is assumed to be a constant for a given flight.

3.4.2 Problem Formulation

Without loss of generality, the inertial coordinate frame is rotated so that the p_1 axis is aligned with the wind velocity $\mathbf{v}_{a_0}$ at the starting position, and the p_2 axis is aligned with the shear vector $\mathbf{w}_0$. We solve the problem in this wind frame, then transform the optimal trajectory back to the initial frame. In the wind frame, the wind shear can be characterized by a scalar w so that the wind velocity at each position is

$$\begin{bmatrix} v_{a1} \\ v_{a2} \\ v_{a3} \end{bmatrix} = \begin{bmatrix} v_{a_{10}} + w\left(p_2 - p_2(t_0)\right) \\ 0 \\ 0 \end{bmatrix} \tag{80}$$

where $v_{a_{10}} = |\mathbf{v}_{a_0}|$.
The system dynamics are

$$\dot{\mathbf{x}} = \begin{bmatrix} \dot{\mathbf{p}} \\ \dot{\mathbf{v}} \end{bmatrix} = \begin{bmatrix} \mathbf{v} \\ \frac{1}{m}\left[\mathbf{T} - k_d\left(\mathbf{v} - \mathbf{v_a}\right)\right] - \mathbf{g} \end{bmatrix} \tag{81}$$

where $\mathbf{T}$ is the thrust and $\mathbf{g}$ is the gravitational acceleration. Note that one also needs to transform the coordinate of the gravity vector and boundary state values.
The optimal control problem is

$$\begin{aligned} J = \min_{\mathbf{T}} \quad & \int_{t_0}^{t_f} \frac{1}{2}\mathbf{T}^T\mathbf{T} + C_I dt \\ s.t. \quad & (80), (81) \\ & \mathbf{x}\left(t_0\right) = \mathbf{x}_0 \\ & \mathbf{x}(t_f) = \mathbf{x}_f \end{aligned} \tag{82}$$

where C_I, denoted as the cost index, is the ratio of cost of time to cost of control effort.

3.5 Problem Solution

We apply the Pontryagin Maximum Principle (PMP) to this problem following the same procedure in section 3.2. The main result of this section is stated next.

3.5.1 Optimal Trajectory Formula

Theorem 3.5.1 *The optimal flight trajectory for problem* (82) *is*

$$\begin{aligned}
p_1 =&\frac{C_1}{2k_d^2}\left(\frac{w^2}{3}t^3-\frac{mw^2}{k_d}t^2+\frac{2m^2w^2}{k_d^2}t-2t\right)-\frac{C_2m}{4k_d^3}\left(w^2t-\frac{3mw^2}{k_d}+\frac{2k_d}{m}\right)e^{\frac{k_d}{m}t}\\
&-\frac{C_3w}{k_d^2}\left(\frac{t^2}{2}-\frac{m}{k_d}t\right)-\frac{C_4wm}{4k_d^3}e^{\frac{k_d}{m}t}+\frac{C_5wm}{k_d}\left(t+\frac{m}{k_d}\right)e^{-\frac{k_d}{m}t}+C_6wt\\
&-\frac{C_{11}m}{k_d}e^{-\frac{k_d}{m}t}+C_{12}-\frac{mg_2w}{k_d}\left(\frac{t^2}{2}-\frac{m}{k_d}t\right)+\left(v_{a_{10}}-wp_2(t_0)-\frac{mg_1}{k_d}\right)t \qquad (83)\\
p_2 =&\frac{C_1w}{2k_d^2}t^2-\frac{C_2w}{2k_d^2}(t-\frac{3m}{2k_d})e^{\frac{k_d}{m}t}-\frac{C_3}{k_d^2}t-\frac{C_4}{2k_d^2}e^{\frac{k_d}{m}t}-\frac{C_5m}{k_d}e^{-\frac{k_d}{m}t}+C_6-\frac{mg_2}{k_d}t\\
p_3 =&-\frac{C_7}{k_d^2}t-\frac{C_8}{2k_d^2}e^{\frac{k_d}{m}t}-\frac{C_9m}{k_d}e^{-\frac{k_d}{m}t}+C_{10}-\frac{mg_3}{k_d}t
\end{aligned}$$

And the optimal cost for a given flight time t_f is

$$J^* = J'(t_f) - J'(t_0) \qquad (84)$$

where

$$\begin{aligned}
J'(t) =& \frac{1}{2}\Bigg[\frac{C_1^2}{k_d^2}\left(\frac{w^2}{3}t^3+\frac{w^2m}{k_d}t^2+\frac{w^2m^2}{k_d^2}t+t\right)+\frac{C_2^2}{2mk_d}\left(w^2t^2-\frac{w^2m}{k_d}t+\frac{w^2m^2}{2k_d^2}+1\right)E(2t)\\
&+\frac{C_3^2}{k_d^2}t+\frac{C_4^2}{2mk_d}E(2t)-\frac{2C_1C_2}{k_d^2}\left(w^2t^2-\frac{w^2m}{k_d}t+\frac{w^2m^2}{k_d^2}-1\right)E(t)-\frac{C_1C_3w}{k_d^2}\left(t^2+\frac{2m}{k_d}t\right)\\
&-\frac{2C_1C_4w}{k_d^2}tE(t)+\frac{2C_2C_3w}{k_d^2}\left(t-\frac{m}{k_d}\right)E(t)+\frac{C_2C_4w}{mk_d}\left(t-\frac{m}{2k_d}\right)E(2t)+\frac{2C_3C_4}{k_d^2}E(t)\\
&+\frac{C_7^2}{k_d^2}t+\frac{C_8^2}{2mk_d}E(2t)+\frac{2C_7C_8}{k_d^2}E(t)\Bigg]+C_It
\end{aligned} \qquad (85)$$

where p_i is the position coordinate for $i = 1, 2, 3$, k_d is the drag coefficient defined in (79)*, m is the mass, and C_1 to C_{12} are coefficients calculated from the boundary values*

$$\begin{bmatrix} \mathbf{x}(t_0) \\ \mathbf{x}(t_f) \end{bmatrix} = \begin{bmatrix} \mathbf{x}_0 \\ \mathbf{x}_f \end{bmatrix} \qquad (86)$$

and $E(t) = e^{\frac{k_d}{m}t}$.

Proof: The Hamiltonian of (82) is

$$H = \frac{1}{2}|\mathbf{T}|^2 + C_I + \lambda_1\dot{p_1} + \lambda_2\dot{p_2} + \lambda_3\dot{p_3} + \lambda_4\dot{v_1} + \lambda_5\dot{v_2} + \lambda_6\dot{v_3} \qquad (87)$$

From PMP, we have

$$\frac{\partial H}{\partial \mathbf{T}} = \begin{bmatrix} T_1 \\ T_2 \\ T_3 \end{bmatrix} + \frac{1}{m}\begin{bmatrix} \lambda_4 \\ \lambda_5 \\ \lambda_6 \end{bmatrix} = \begin{bmatrix} 0 \\ 0 \\ 0 \end{bmatrix} \qquad (88)$$

$$\mathbf{T} = \frac{1}{m}[-\lambda_4, -\lambda_5, -\lambda_6]^T \tag{89}$$

Replacing (81) and (89) into (87) yields

$$\begin{aligned} H = &- \frac{1}{2m^2}(\lambda_4^2 + \lambda_5^2 + \lambda_6^2) + \lambda_1 v_1 + \lambda_2 v_2 + \lambda_3 v_3 \\ &- \frac{k_d}{m}\left[\lambda_4(v_1 - v_{a1}) + \lambda_5(v_2 - v_{a2}) + \lambda_6(v_3 - v_{a3})\right] \\ &- (\lambda_4 g_1 + \lambda_5 g_2 + \lambda_6 g_3) + C_I \end{aligned} \tag{90}$$

From the Hamilton's equations and considering (80), we get

$$\frac{\partial H}{\partial \mathbf{p}} = \frac{k_d}{m}\begin{bmatrix} 0 \\ \lambda_4 w \\ 0 \end{bmatrix} = \begin{bmatrix} -\dot{\lambda}_1 \\ -\dot{\lambda}_2 \\ -\dot{\lambda}_3 \end{bmatrix} \tag{91}$$

$$\frac{\partial H}{\partial \mathbf{v}} = \begin{bmatrix} \lambda_1 - \frac{k_d}{m}\lambda_4 \\ \lambda_2 - \frac{k_d}{m}\lambda_5 \\ \lambda_3 - \frac{k_d}{m}\lambda_6 \end{bmatrix} = \begin{bmatrix} -\dot{\lambda}_4 \\ -\dot{\lambda}_5 \\ -\dot{\lambda}_6 \end{bmatrix} \tag{92}$$

Let

$$\lambda_1 = C_1 \tag{93}$$

Then

$$\dot{\lambda_4} - \frac{k_d}{m}\lambda_4 = -C_1 \tag{94}$$

$$\lambda_4 = \frac{C_1 m}{k_d} + C_2 e^{\frac{k_d}{m}t} \tag{95}$$

Replacing (95) in the fourth equation of (81) together with (89) yields

$$\dot{v}_1 = \frac{1}{m}\left[-\frac{C_1}{k_d} - \frac{C_2}{m}e^{\frac{k_d}{m}t} - k_d(v_1 - v_{a_1})\right] - g_1 \tag{96}$$

Recalling (80) we obtain

$$\dot{v}_1 + \frac{k_d}{m}v_1 = -\frac{C_1}{mk_d} - \frac{C_2}{m^2}e^{\frac{k_d}{m}t} + \frac{k_d}{m}(v_{a_{10}} + wp_2 - wp_{20}) - g_1 \tag{97}$$

Replacing (95) into (91) and solving leads to

$$\lambda_2 = -C_1 wt - C_2 w e^{\frac{k_d}{m}t} + C_3 \tag{98}$$

Replacing λ_2 into (92) yields

$$\dot{\lambda_5} - \frac{k_d}{m}\lambda_5 = C_1 wt + C_2 w e^{\frac{k_d}{m}t} - C_3 \tag{99}$$

whose solution is

$$\lambda_5 = -\frac{C_1 w m}{k_d}\left(t + \frac{m}{k_d}\right) + C_2 w t e^{\frac{k_d}{m}t} + \frac{m}{k_d}C_3 + C_4 e^{\frac{k_d}{m}t} \tag{100}$$

Replacing (100) in the fifth equation of (81) results in

$$\dot{v_2} + \frac{k_d}{m}v_2 = \frac{C_1 w}{m k_d}\left(t + \frac{m}{k_d}\right) - \frac{C_2 w}{m^2}t e^{\frac{k_d}{m}t} - \frac{C_3}{m k_d} - \frac{C_4}{m^2}e^{\frac{k_d}{m}t} - g_2 \tag{101}$$

which yields by successive integration

$$v_2 = \frac{C_1 w}{k_d^2}t - \frac{C_2 w}{2 m k_d}\left(t - \frac{m}{2k_d}\right)e^{\frac{k_d}{m}t} - \frac{C_3}{k_d^2} - \frac{C_4}{2 m k_d}e^{\frac{k_d}{m}t} + C_5 e^{-\frac{k_d}{m}t} - \frac{m g_2}{k_d} \tag{102}$$

$$p_2 = \frac{C_1 w}{2k_d^2}t^2 - \frac{C_2 w}{2k_d^2}\left(t - \frac{3m}{2k_d}\right)e^{\frac{k_d}{m}t} - \frac{C_3}{k_d^2}t - \frac{C_4}{2k_d^2}e^{\frac{k_d}{m}t} - \frac{C_5 m}{k_d}e^{-\frac{k_d}{m}t} + C_6 - \frac{m g_2}{k_d}t \tag{103}$$

Integrating (97) yields

$$\begin{aligned} v_1 =& \frac{C_1}{2k_d^2}\left(w^2 t^2 - \frac{2mw^2}{k_d}t + \frac{2m^2 w^2}{k_d^2} - 2\right) - \frac{C_2}{4k_d^2}\left(w^2 t - \frac{2mw^2}{k_d} + \frac{2k_d}{m}\right)e^{\frac{k_d}{m}t} \\ & - \frac{C_3 w}{k_d^2}\left(t - \frac{m}{k_d}\right) - \frac{C_4 w}{4k_d^2}e^{\frac{k_d}{m}t} - C_5 w t e^{-\frac{k_d}{m}t} + C_6 w + C_{11}e^{-\frac{k_d}{m}t} \\ & - \frac{m g_2 w}{k_d}\left(t - \frac{m}{k_d}\right) + \left(v_{a_{10}} - w p_2(t_0) - \frac{m g_1}{k_d}\right) \end{aligned} \tag{104}$$

Integrating we get p_1 in (83). Let

$$\lambda_3 = C_7 \tag{105}$$

From (92) and (105)

$$\lambda_6 = \frac{C_7 m}{k_d} + C_8 e^{\frac{k_d}{m}t} \tag{106}$$

Replacing (106) in the third equation of (81) and integrating twice yields

$$v_3 = -\frac{C_7}{k_d^2} - \frac{C_8}{2 m k_d}e^{\frac{k_d}{m}t} + C_9 e^{-\frac{k_d}{m}t} - \frac{m g_3}{k_d} \tag{107}$$

$$p_3 = -\frac{C_7}{k_d^2}t - \frac{C_8}{2k_d^2}e^{\frac{k_d}{m}t} - \frac{C_9 m}{k_d}e^{-\frac{k_d}{m}t} + C_{10} - \frac{m g_3}{k_d}t \tag{108}$$

From (89), (95), (100), (106), we get

$$\begin{bmatrix} T_1 \\ T_2 \\ T_3 \end{bmatrix} = -\begin{bmatrix} \frac{C_1}{k_d} + \frac{C_2}{m}E(t) \\ -\frac{C_1 w}{k_d}\left(t + \frac{m}{k_d}\right) + \frac{C_2 w}{m}t E(t) + \frac{C_3}{k_d} + \frac{C_4}{m}E(t) \\ \frac{C_7}{k_d} + \frac{C_8}{m}E(t) \end{bmatrix} \tag{109}$$

Replacing (109) into the cost function in (82) and integrating, expression (84) is obtained. Q.E.D.

Remark 3.5.2 *Letting*

$$v_{a_{10}} = w = g_1 = g_2 = 0 \tag{110}$$

yields

$$\begin{aligned} p_1 &= -\frac{C_1}{k_d^2}t - \frac{C_2}{2k_d^2}e^{\frac{k_d}{m}t} - \frac{C_{11}m}{k_d}e^{-\frac{k_d}{m}t} + C_{12} \\ p_2 &= -\frac{C_3}{k_d^2}t - \frac{C_4}{2k_d^2}e^{\frac{k_d}{m}t} - \frac{C_5m}{k_d}e^{-\frac{k_d}{m}t} + C_6 \\ p_3 &= -\frac{C_7 + mg_3k_d}{k_d^2}t - \frac{C_8}{2k_d^2}e^{\frac{k_d}{m}t} - \frac{C_9m}{k_d}e^{-\frac{k_d}{m}t} + C_{10} \end{aligned} \tag{111}$$

which matches with Theorem 3.2.1.

Remark 3.5.3 *We can add a positive shear vector with increasing altitude to emulate the drag reduction caused by air density dropping.*

3.5.2 Optimal Flight Time and Peak Thrust Constraint

Since the optimal cost is derived as a function of the flight time in equation (84). A static optimization technique (such as the one described in [76]) is applied to (84) to find the optimal flight time. A peak thrust constraint is imposed as a hard penalty to a number of time instants within the flight time. The pseudocode for this procedure is as follows

Algorithm 5 solution procedure

get $\mathbf{x}_0, \mathbf{x}_f, \mathbf{v}_{a_0}, \mathbf{w}_0$;
set C_I;
transform the coordinates as stated in section 3.4.2;
compute the optimal time $t_{op} = \text{fmin}\big(\text{cost}(t_f)\big)$;
compute the coefficients $C_1 \sim C_{12}$ with (86);
compute the reference position for each time instant with (83);

function COST(t_f)
    compute the coefficients $C_1 \sim C_{12}$ with (86);
    compute the total cost J with (84);
    for t=linspace($t_0, t_f, 100$) **do**
        if $|\mathbf{T}(t)| > T_{max}$ **then**
            $J = J + Inf$;
            Break;
        end if
    end for
    return J;
end function

3.5.3 Optimal Trajectory in Time-dependent Wind

Corollary 3.5.4 *If a time-dependent wind component $w(t)$ is included such that the wind velocity becomes*

$$\begin{bmatrix} v_{a1} \\ v_{a2} \\ v_{a3} \end{bmatrix} = \begin{bmatrix} v_{a_{10}} + w\left(p_2 - p_2(t_0)\right) + w_1(t) \\ w_2(t) \\ w_3(t) \end{bmatrix} \tag{112}$$

the optimal trajectory is

$$p_i'(t) = p_i(t) + \int_{t_0}^{t} \frac{k_d \int_{t_0}^{s} w_i(\tau) e^{\frac{k_d}{m}\tau} d\tau}{m e^{\frac{k_d}{m}s}} ds \tag{113}$$

where $p_i(t)$ is the previous solution as written in (83).

Proof: Following the previous proof, the Hamiltonian is

$$H = \frac{1}{2}\mathbf{T}^2 + C_I + \begin{bmatrix} \lambda_1 \\ \lambda_2 \\ \lambda_3 \end{bmatrix}^T \mathbf{v} + \begin{bmatrix} \lambda_4 \\ \lambda_5 \\ \lambda_6 \end{bmatrix}^T \dot{\mathbf{v}} \tag{114}$$

The optimal thrust is still

$$\mathbf{T} = \frac{1}{m}[-\lambda_4, -\lambda_5, -\lambda_6]^T \tag{115}$$

Since the added term is solely a function of time, the costates dynamics are unchanged.

$$\frac{\partial H}{\partial \mathbf{p}} = \frac{k_d}{m}\begin{bmatrix} 0 \\ \lambda_4 w \\ 0 \end{bmatrix} = \begin{bmatrix} -\dot{\lambda}_1 \\ -\dot{\lambda}_2 \\ -\dot{\lambda}_3 \end{bmatrix} \tag{116}$$

$$\frac{\partial H}{\partial \mathbf{v}} = \begin{bmatrix} \lambda_1 - \frac{k_d}{m}\lambda_4 \\ \lambda_2 - \frac{k_d}{m}\lambda_5 \\ \lambda_3 - \frac{k_d}{m}\lambda_6 \end{bmatrix} = \begin{bmatrix} -\dot{\lambda}_4 \\ -\dot{\lambda}_5 \\ -\dot{\lambda}_6 \end{bmatrix} \tag{117}$$

Hence, the same equations for λ_i are obtained as (95), (100), (106). Take v_1 for example: the dynamics of velocity becomes

$$\begin{aligned} \dot{v}_1(t) + \frac{k_d}{m}v_1(t) &= -\frac{C_1}{mk_d} - \frac{C_2}{m^2}e^{\frac{k_d}{m}t} + \frac{k_d}{m}\left(v_{a_{10}} + wp_2(t) - wp_{20} + w_1(t)\right) - g_1 \\ &= RHS + \frac{k_d}{m}w_1(t) \end{aligned} \tag{118}$$

where RHS stands for the right hand side of (97). Denote the solution of velocity and position as $v'$and p' to distinguish from the previous formula. Integrating yields

$$v_1'(t) = v_1(t) + \frac{k_d \int_{t_0}^{t} w_1(\tau)e^{\frac{k_d}{m}\tau}d\tau}{me^{\frac{k_d}{m}t}} \tag{119}$$

where $v_1(t)$ is the previous solution written in (104). The optimal trajectory is obtained by another integration as

$$p_1'(t) = p_1(t) + \int_{t_0}^{t} \frac{k_d \int_{t_0}^{s} w_1(\tau)e^{\frac{k_d}{m}\tau}d\tau}{me^{\frac{k_d}{m}s}}ds \tag{120}$$

where $p_i(t)$ is the previous solution as written in (83). This result applies to all the three dimensions. Q.E.D.

3.6 Simulation Results

The DJI Phantom 4 Pro [78] is chosen for the simulation with the parameters $m = 1.388kg, l = 0.35m$ (required for k_d as in section 3.3), $T_{max} = 50N$. The air density $\rho_{air} = 1.225kg/m^3$ is chosen at sea level from [4]. Assuming that hovering rotorcraft are rough spherical objects, the k_d is calculated with a drag coefficient $C_D = 0.3$ chosen from [77] and with v_{avg} obtained by dividing the flight distance with time. The cost index is $C_I = 1$.

The boundary conditions and wind field are

$x_0 = [0, 0, 1, 3, -1, 2]$;

$x_f = [3150, 270, 57, 0, 0, 0]$;

$v_{a_0} = [2, \sqrt{5}, 0]$;

$w_0 = 0.01[-\sqrt{5}, 2, \sqrt{7}]/4$;

The parameters for this simulation are collected in Table 5.

Table 5: Simulation parameters

Parameter	Value
p_0 (m)	0,0,1
v_0 (m/s)	3,-1,2
p_f (m)	3150,270,57
v_f (m/s)	0,0,0
v_{a_0} (m/s)	$2,\sqrt{5},0$
w_0 $(1/s)$	$0.01\times[-\sqrt{5},2,\sqrt{7}]/4$
C_I	1
m (kg)	1.388
l (m)	0.35
C_D	0.3
ρ_{air} (kg/m^3)	1.225
g (m/s^2)	9.8
T_{max} (N)	50

In Fig. 16, the blue arrows indicate the wind field. The black curve represents the optimal flight path obtained by the method proposed in this section, while the magenta is the path in absence of wind. It is interesting to see that even a $3m/s$ wind with $0.01/s$ shear results in such a big difference in the flight path. The corresponding velocity and thrust over time are shown in Fig. 17 and Fig. 18. In these plots, the solid lines refer to the magnitude while the other three lines indicate the three coordinates. The disparities in the velocity profiles of the trajectories planned with and without wind are clearly shown. In absence of wind, a large portion of the flight is steady flight. While in presence of wind, the aircraft maneuvers in favor of wind and also satisfies the boundary states. The thrust stays well beneath the upper limit. In absence of wind, the optimal flight time is $152.1s$ and the total cost is 1.910×10^4. In presence of the constant wind shear, the optimal time is $158.9s$ and the cost is 2.014×10^4. If the trajectory that was planned neglecting wind is flown in the same wind field, the actual thrust is plotted in Fig. 19 and the actual cost is 2.101×10^4. Therefore, a 4.3% improvement is achieved with the solution provided in this section. To compare the two trajectories planned considering and neglecting wind in the same wind field, the optimal flight times and total cost for two sets of wind parameters are

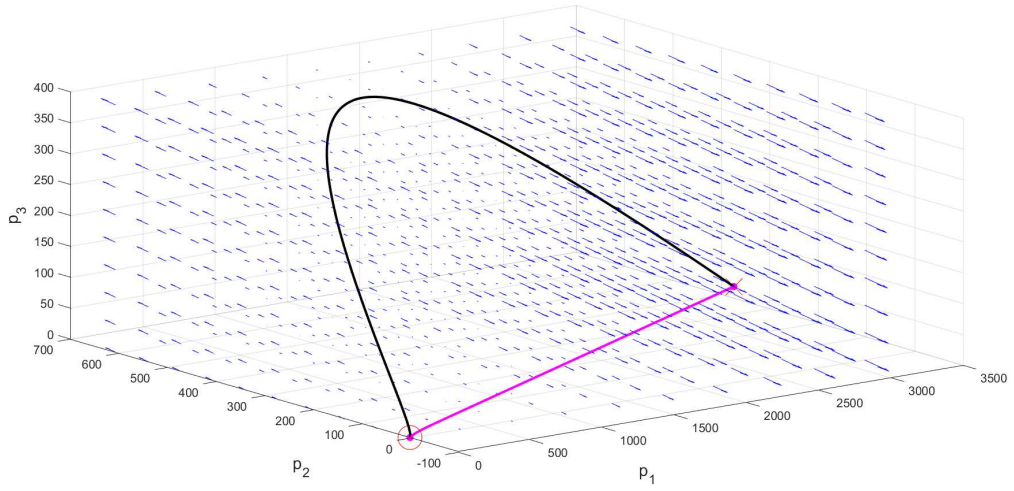

Figure 16: 3D flight trajectory in wind

collected in Table 6. Setting 1: $v_{a_0} = [2, \sqrt{5}, 0]; w_0 = 0.01[-\sqrt{5}, 2, \sqrt{7}]/4$.
Setting 2: $v_{a_0} = [2, \sqrt{5}, 0]; w_0 = 0.1[-\sqrt{5}, 2, \sqrt{7}]/4$.

Table 6: Total cost

Cost	Trajectory neglecting wind	Trajectory considering wind
Setting 1	2.101×10^4	2.014×10^4
Setting 2	1.254×10^5	3.779×10^4

If the magnitude of shear w is $0.1/s$, the cost neglecting wind is 1.254×10^5, while that considering wind is 3.779×10^4. Therefore, the cost is 2.3 times higher if the wind is neglected during trajectory planning. In order to obtain a Pareto analysis, the maximum thrust is set at $100N$ to allow for a larger diversity of possible flight times. The Pareto trade-off curve of this flight is depicted in Fig. 20, which illustrates the trade-off between the flight time and control effort. The larger the C_I, the smaller the flight time and the higher the control effort cost.

3.7 Conclusions

In the first half of this chapter, we presented an analytical solution of the optimal trajectory trading-off control effort and flight time. The approach allowed arbitrary boundary conditions, and both fixed and free flight times. An approximate solution for long haul flights was derived so as to reduce the computational time. A characteristic term was proposed to determine whether to use the analytical solution or the approximation. The

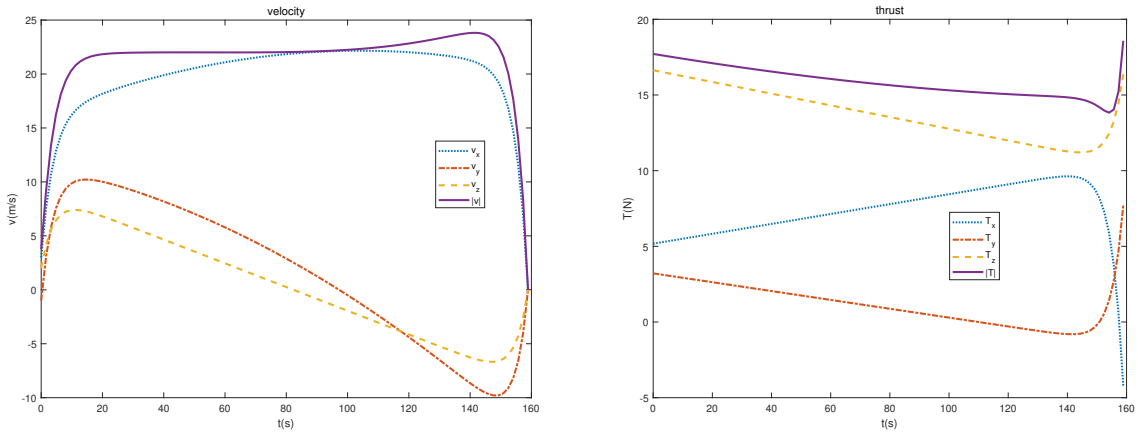

Figure 17: Velocity and thrust plots with wind

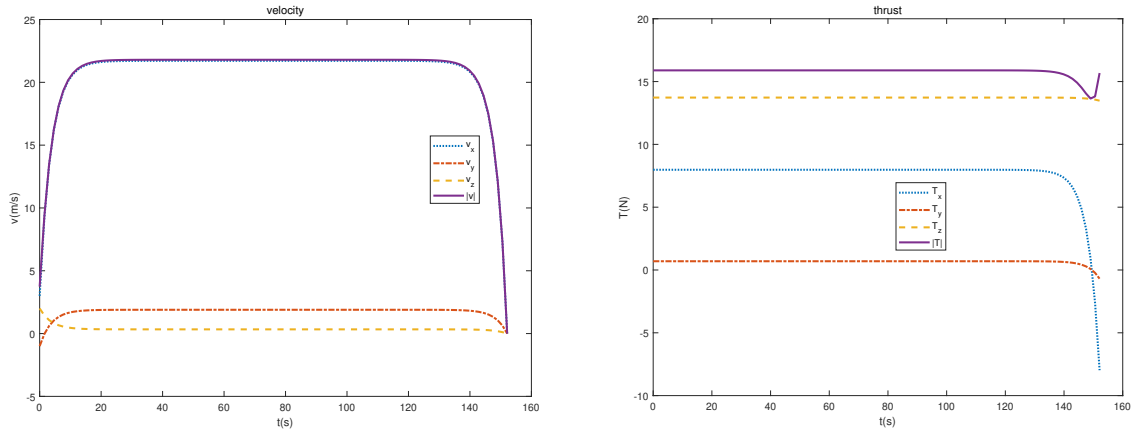

Figure 18: Velocity and thrust plots without wind

method was extended to respect peak velocity constraints. Additionally, the optimal trajectory in a constant wind shear field was presented and a peak thrust constraint was enforced. The Pareto optimal trade-off curve provides a helpful tool to select the cost index C_I in practice.

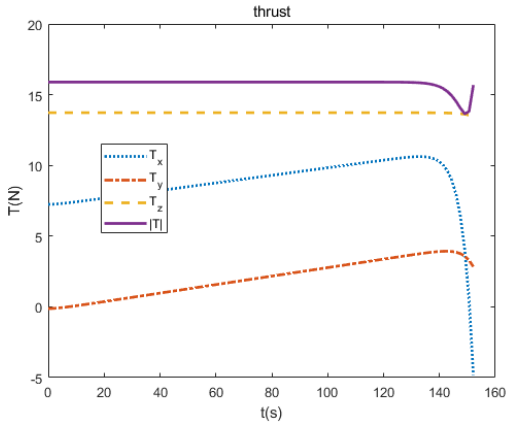

Figure 19: Actual thrust in wind

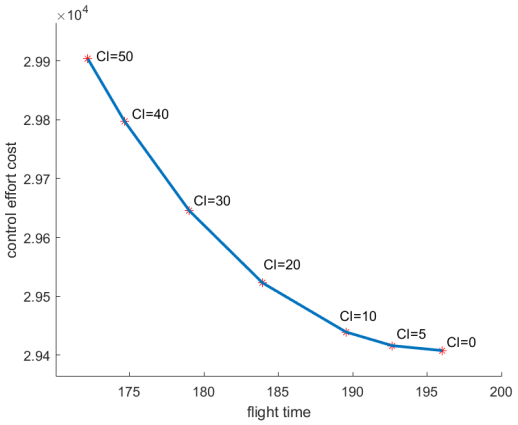

Figure 20: Pareto tradeoff

Chapter 4

DOC-optimal Longitudinal Trajectory for Electric Fixed-wing Aircraft: A Hybrid Optimal Control Approach

4.1 Introduction

This chapter presents the optimal longitudinal trajectory for electric fixed-wing aircraft trading-off two costs: energy consumption and flight time costs. Compared to the open literature, the contributions of this chapter are:

- the trajectory planning is formulated as a hybrid optimal control problem (HOCP) to find the optimal trajectory for all phases of flight,
- the proposed solution does not require an initial guess of the costate, which saves computational time,
- altitude-dependent along-track horizontal wind is considered so that the solution can yield the optimal flight profile in the presence of wind,
- a maximum Mach number constraint and a maximum lift coefficient constraint are enforced in a suboptimal solution to prevent results that are practically infeasible.

The structure of this chapter is as follows. Section 4.2 presents the problem formulation, while the detailed solution of the optimal trajectory appears in section 4.3. Simulation results are presented in section 4.4. Concluding remarks are stated in section 4.5.

4.2 Problem Formulation

4.2.1 Problem description

This chapter finds the optimal longitudinal trajectory for an electric fixed-wing aircraft trading-off energy consumption and flight time between two positions $[x_0, z_0]$ and $[x_f, z_f]$, where x_0, z_0 are the initial horizontal and vertical position respectively.

4.2.2 Assumptions

1. The trajectory consists of climb, cruise and descent phases. Maximum thrust (T_{max}) is used for climb, idle thrust (T_{min}) for descent, constant altitude (h_c) for cruise.

2. The component of thrust perpendicular to the velocity is negligible compared to weight.

3. The gravity is assumed constant.

4. The inertial force is neglected compared to drag, thrust and the component of weight aligned with the velocity.

5. The centrifugal force is neglected compared to weight and lift.

6. The aircraft is flying at a Mach number that is lower than the drag divergence Mach number (M_D).

7. Small angle assumptions hold for the flight path angle γ

$$cos\gamma \approx 1; sin\gamma \approx \gamma; tan\gamma \approx \gamma \tag{121}$$

8. Propulsion efficiency η is constant so that the battery charge rate of change is

$$\dot{Q} = \frac{T v_G}{\eta} \tag{122}$$

   where T is thrust, and v_G is ground speed.

9. The velocity v is continuous.

10. The drag verifies $D \neq T_{max}$, $D \neq T_{min}$.

4.2.3 Flight dynamics

For mass m, gravity g, path angle γ, radius of curvature R, acceleration a, the flight dynamics [80] in accordance with the assumptions 2 to 7 are

$$L = m(gcos\gamma + \frac{v_G^2}{R}) \approx mg \tag{123}$$

$$T = D + m(gsin\gamma + a) \approx D + mg\gamma \tag{124}$$

where L is lift, and the ground speed v_G is expressed as a function of the airspeed v and wind speed v_w as

$$v_G = v + v_w \tag{125}$$

In (124), D is the drag expressed as

$$D = D(v, z) = \frac{1}{2}\rho(z)v^2SC_D \tag{126}$$

where ρ is the air density, S is the characteristic surface area, and C_D is the drag coefficient. We consider a parabolic drag coefficient

$$C_D = C_{D0} + k_d C_L^2 \tag{127}$$

where C_{D0}, k_d are constant, and C_L is the lift coefficient such that

$$L = \frac{1}{2}\rho v^2 S C_L \tag{128}$$

Considering (123), (127) and (128), we get

$$C_D = C_{D0} + k_d\left(\frac{2mg}{\rho v^2 S}\right)^2 \tag{129}$$

To make the optimal control problem more realistic to solve, we take the air density data (part of which is shown in Table 7) from the US Standard Atmosphere [4], and fit a function for the relationship between air density ρ (kg/m^3) and altitude z (m) as

$$\rho(z) = 4.098e^{-\left(\frac{z+2.608e+04}{2.374e+04}\right)^2} \tag{130}$$

This formula is found using Matlab Curve Fitting Toolbox by solving the parameters of an exponential function with a second order exponent that minimizes the mean squared error. The second order exponential function yields smaller error than the first order exponential function and is simpler than the higher order counterparts. It is more suitable for the problem formulation than the well known two-part formulas [81]. The fitted curve matches the standard values as shown in Fig. 21.

Table 7: Standard air density [4]

altitude (m)	air density (kg/m^3)	speed of sound (m/s)
-1000	1.347	344.1
0	1.225	340.3
1000	1.112	336.4
2000	1.007	332.5
3000	0.9093	328.6
4000	0.8194	324.6
5000	0.7364	320.5
6000	0.6601	316.5
7000	0.5900	312.3
8000	0.5258	308.1
9000	0.4671	303.8
10000	0.4135	299.5
15000	0.1948	295.1
20000	0.08891	295.1

4.2.4 System dynamics

Since the thrust is constrained by the flight rules such as assumption 1, we take the speed as the control variable. The system dynamics are

$$\frac{d}{dt}\begin{bmatrix} x \\ z \end{bmatrix} = \begin{bmatrix} v_G cos\gamma \\ v_G sin\gamma \end{bmatrix} \tag{131}$$

We choose the horizontal position x as the independent variable, so that the state is solely z. Considering (121) and (124), the system dynamics are

$$\frac{dz}{dx} = \gamma = \frac{T - D(v,z)}{mg} \tag{132}$$

where

$$T = \begin{cases} T_{max}, & \text{climb} \\ D(v,z), & \text{cruise} \\ T_{min}, & \text{descent} \end{cases} \tag{133}$$

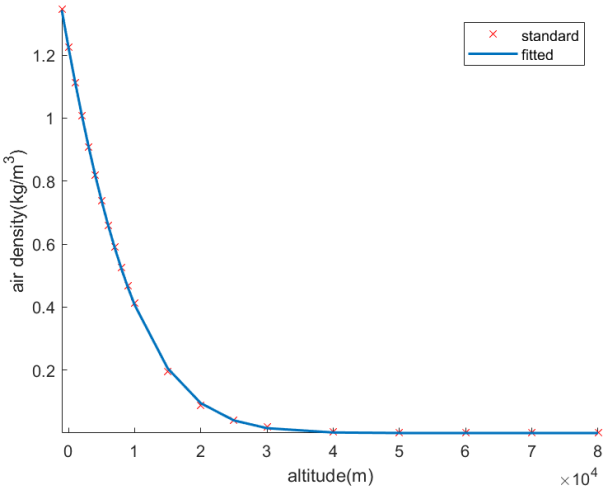

Figure 21: Air density interpolation

4.2.5 Optimal control problem

The optimal control problem is

$$\begin{aligned} J = \min_{v} \quad & \int_{x_0}^{x_f} \frac{T}{\eta} + \frac{C_I}{v + v_w(z)} dx \\ s.t. \quad & (132), (133), (126), (129) \\ & z\left(x_0\right) = z_0 \\ & z(x_f) = z_f \\ & v \in C^0 \end{aligned} \tag{134}$$

where C^0 is the set of continuous functions, and C_I is denoted as the cost index, which is the ratio of the cost of time to the cost of energy consumption. We apply the Pontryagin's Minimum Principle (PMP) [74] and Hybrid Optimal Control (HOC) [82] to this problem.

4.3 Problem Solution

Before solving the problem formulated in (134), we briefly review the optimality conditions for hybrid optimal control.

4.3.1 Hybrid optimal control theory

According to [82], for each phase of flight q with Hamiltonian H_q, the necessary conditions are

$$\frac{\partial H_q}{\partial v} = 0 \tag{135}$$

$$\dot{\lambda} = -\frac{\partial H_q}{\partial z} \tag{136}$$

$$\lambda_{q-1}(x_q^-) = \lambda_q(x_q) \tag{137}$$

$$H_{q-1}(x_q^-) = H_q(x_q) \tag{138}$$

where x_q is the switching instant from phase $q-1$ to phase q, and x_q^- is the left limit of x_q.

4.3.2 Optimal trajectory for a given cruising altitude

Theorem 4.3.1 *The optimal airspeed for a given cruising altitude is a solution of*

$$0 = \begin{cases} -\frac{C_I}{(v+v_w)^2} + \frac{\lambda}{mg}\left(-\rho S C_{D0} v + \frac{4m^2g^2k_d}{\rho S v^3}\right), & \textit{climb} \\ -\frac{C_I}{(v+v_w)^2} + \frac{1}{\eta}\left(\rho S C_{D0} v - \frac{4m^2g^2k_d}{\rho S v^3}\right), & \textit{cruise} \\ -\frac{C_I}{(v+v_w)^2} + \frac{\lambda}{mg}\left(-\rho S C_{D0} v + \frac{4m^2g^2k_d}{\rho S v^3}\right), & \textit{descent} \end{cases} \tag{139}$$

At the top of climb x_c and the top of descent x_d, the values of the costate are

$$\lambda(x_c-) = \lambda(x_d) = -\frac{mg}{\eta} \tag{140}$$

Proof: For this problem, we consider the flight consisting of three phases, which are

$$\begin{aligned} &\text{climb: } q = 1 \\ &\text{cruise: } q = 2 \\ &\text{descent: } q = 3 \end{aligned} \tag{141}$$

Climb occurs for $x \in [x_0, x_c)$, cruise occurs for for $x \in [x_c, x_d)$, and descent corresponds to $x \in [x_d, x_f]$. The Hamiltonians for each phase are

$$\begin{aligned} H_1 &= \frac{T_{max}}{\eta} + \frac{C_I}{v+v_w} + \lambda\frac{T_{max} - D}{mg} \\ H_2 &= \frac{D}{\eta} + \frac{C_I}{v+v_w} \\ H_3 &= \frac{T_{min}}{\eta} + \frac{C_I}{v+v_w} + \lambda\frac{T_{min} - D}{mg} \end{aligned} \tag{142}$$

According to PMP, the optimal velocity is the solution of

$$\frac{\partial H}{\partial v} = 0 \tag{143}$$

which yields

$$0 = \begin{cases} -\frac{C_I}{(v+v_w)^2} + \frac{\lambda}{mg}\left(-\rho S C_{D0} v + \frac{4m^2g^2k_d}{\rho S v^3}\right), & \text{climb} \\ -\frac{C_I}{(v+v_w)^2} + \frac{1}{\eta}\left(\rho S C_{D0} v - \frac{4m^2g^2k_d}{\rho S v^3}\right), & \text{cruise} \\ -\frac{C_I}{(v+v_w)^2} + \frac{\lambda}{mg}\left(-\rho S C_{D0} v + \frac{4m^2g^2k_d}{\rho S v^3}\right), & \text{descent} \end{cases} \tag{144}$$

The costate dynamics are

$$\begin{aligned}\frac{\partial H}{\partial z} &= -\dot{\lambda} \\ &= \begin{cases} \frac{\lambda}{mg}\left(-\frac{1}{2}SC_{D0}v^2 + \frac{2m^2g^2k_d}{\rho^2Sv^2}\right)\frac{\partial \rho}{\partial z} - \frac{C_I}{(v+v_w)^2}\frac{\partial v_w}{\partial z}, & \text{climb} \\ 0, & \text{cruise} \\ \frac{\lambda}{mg}\left(-\frac{1}{2}SC_{D0}v^2 + \frac{2m^2g^2k_d}{\rho^2Sv^2}\right)\frac{\partial \rho}{\partial z} - \frac{C_I}{(v+v_w)^2}\frac{\partial v_w}{\partial z}, & \text{descent} \end{cases}\end{aligned} \tag{145}$$

The optimal switching (138) yields

$$H_1(x_c-) = H_2(x_c) \tag{146}$$

$$H_2(x_d-) = H_3(x_d) \tag{147}$$

Replacing (142) and enforcing continuity of the velocity at the switching (assumption 9), we get

$$(T_{max} - D)\left(\frac{1}{\eta} + \frac{\lambda(x_c-)}{mg}\right) = 0 \tag{148}$$

$$(T_{min} - D)\left(\frac{1}{\eta} + \frac{\lambda(x_d)}{mg}\right) = 0 \tag{149}$$

From assumption 10,

$$\lambda(x_c-) = \lambda(x_d) = -\frac{mg}{\eta} \tag{150}$$

The left part of (150) is consistent with the necessary condition (137). Q.E.D.

4.3.3 Suboptimal Solution Satisfying Speed Constraints

In order to deal with the speed constraints, we enforce the minimum and maximum constraints on the airspeed at every time step. The cost function is obtained for a cruising altitude h_c. We then optimize over h_c to find the optimal cruising altitude and thus the longitudinal path. Note that a feasible flight envelope for the cruising altitude is set for this optimization. The algorithm to compute the cost given a cruising altitude (h_c) and a cost index (C_I) is as follows:

Algorithm 6 calculating the optimal cost for a cruising altitude

function COST(h_c)

Step 1: get air density $\rho(h_c)$, speed of sound $v_s(h_c)$ from [4] such as Table 7;

Step 2: solve (144) for cruise speed v.

Considering the speed constraints, the feasible cruising speed is

$v_c = max(min(v, M_D v_s(h_c)), v_{min}(h_c))$

Step 3: solve differential equations (132), (145) in climb and descent using the solution of equation (144) as an input, and $z(x_0) = z_0$, $z(x_f) = z_f$, $v(x_c) = v(x_d) = v_c$ to get top of climb (x_c) and top of descent (x_d);

if $x_0 \leq x_c \leq x_d \leq x_f$ **then**

return $J = \int_{x_0}^{x_f} \frac{T}{\eta} + \frac{C_I}{v+v_w(z)} dx$;

else

return $J = \infty$;

end if

end function

To determine the optimal cruising altitude one only has to solve $h^* = argmin(\text{COST}(h))$.

Remark 4.3.2 *The x_c and x_d can be computed using the terminal event of ode45, the integral of the cost is computed using ode45, and h^* is computed using fmincon in Matlab^{TM}.*

4.4 Simulation Results

Table 8 shows the parameters of an Airbus A300 model [83]. The maximum and minimum thrust are scaled as 25% and 2.5% of the weight, respectively. The effects of four factors are studied here: C_I, η, m, and $v_w(z)$. The boundary positions are $[0, 0]$ and $[1000000, 0]$. The default values for the parameters are $C_I = 100000, \eta = 1, v_w(z) = 0m/s$.

4.4.1 Effect of cost index C_I

The simulation results are collected in Table 9. The tradeoff between energy consumption and flight time is depicted in Fig. 22. The bigger is C_I, the more expensive is the time of flight. Therefore, the aircraft tends to fly faster, which implies higher altitude. Also, more energy is consumed.

The optimal trajectories are shown in Fig. 23 for two different values of C_I. The larger is C_I, the higher is the cruising altitude, and the higher is the top speed. The lift coefficients are well below the limit. The peak values of the path angle are almost the same, which

Table 8: Model parameters

Parameter	Value
$S\ (m^2)$	260
$m\ (tons)$	100
C_{D0}	0.0206
k_d	0.0520
CL_{max}	1.4278
$T_{max}\ (N)$	250000
$T_{min}\ (N)$	25000
M_D	0.9
$h_{max}\ (km)$	17
$g\ (kgm/s^2)$	9.8

Table 9: Effect of C_I

C_I	10000	100000	300000
h (m)	0	10637	16220
flight time (s)	10113	6286	5188
energy (GJ)	64.12	64.38	64.52
total cost (GJ)	67.15	66.27	66.08

indicates that the weight component parallel to velocity is dominant for climb and descent.

4.4.2 Effect of efficiency η

The simulation results are listed in Table 10. The higher is the propulsion efficiency, the higher is the cruising altitude, and the lower is the cost for both time and energy. This means that for sufficiently low C_I the plane flies at the minimum altitude, meaning that there is no gain to climb.

Table 10: Effect of efficiency

η	0.4	0.7	1.0
h (m)	0	5681	10637
flight time (s)	10101	7765	6286
energy (GJ)	160.3	91.8	64.4
total cost (GJ)	161.3	92.6	65.0

4.4.3 Effect of mass m

As shown in Table 11, the heavier is the aircraft, the faster and higher it flies, but more energy is required. The aircraft flies much faster at higher altitude to compensate for the

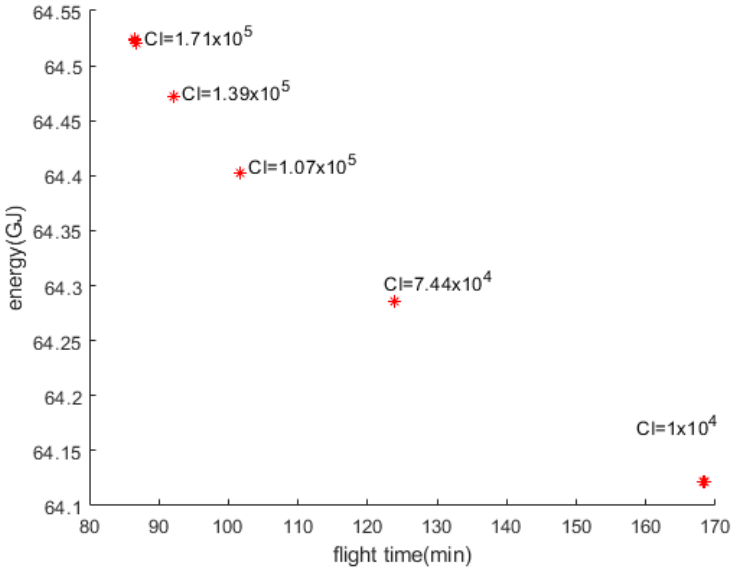

Figure 22: Effect of C_I

drop in air density.

Table 11: Effect of mass

m (t)	60	90	120
h (m)	3471	9328	12685
flight time (s)	11103	7005	5293
energy (GJ)	38.6	58.0	77.2
total cost (GJ)	39.8	58.7	77.7

4.4.4 Effect of along-track horizontal wind $v_w(z)$

The wind profile is shown in Fig. 24, which is an approximation to the jet stream. The differences in the optimal trajectories with and without wind are shown in Fig. 25. The aircraft is able to find the optimal cruising altitude to take advantage of the wind. The airspeeds are similar for the two flights, although there is a subtle difference in the lift coefficients. In absence of wind, the flight time is 1.75 hours, whereas the flight time with wind is 1.52 hours.

4.5 Conclusions

This chapter provided an analytical solution for the longitudinal trajectory which optimizes a trade-off between the energy consumption and flight time for electric fixed-wing

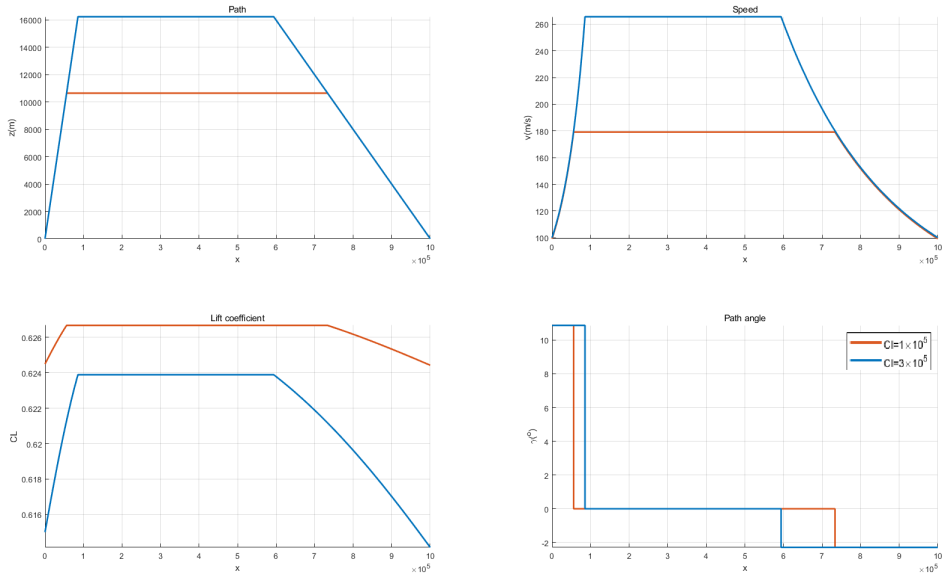

Figure 23: Optimal trajectory for different values of C_I, $C_I = 1 \times 10^5$ for the red line, $C_I = 3 \times 10^5$ for the blue line

aircraft. The approach used hybrid optimal control theory to obtain the optimal trajectory for the whole flight instead of for each phase separately. The solution did not require an initial guess of the costate, which saved computational time. To satisfy the velocity and lift coefficient constraints, a suboptimal numerical solution was proposed to find the cruising altitude. Altitude-dependent along-track horizontal wind was incorporated to find the longitudinal path and speed profiles. The effects of four factors, namely cost index C_I, efficiency η, mass m, and wind velocity $v_w(z)$ were analyzed. The higher were C_I, η, m, the higher and faster the airplane flew.

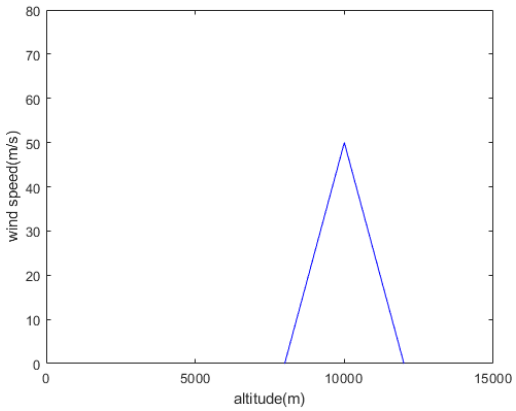

Figure 24: Vertical profile of along-track wind speed

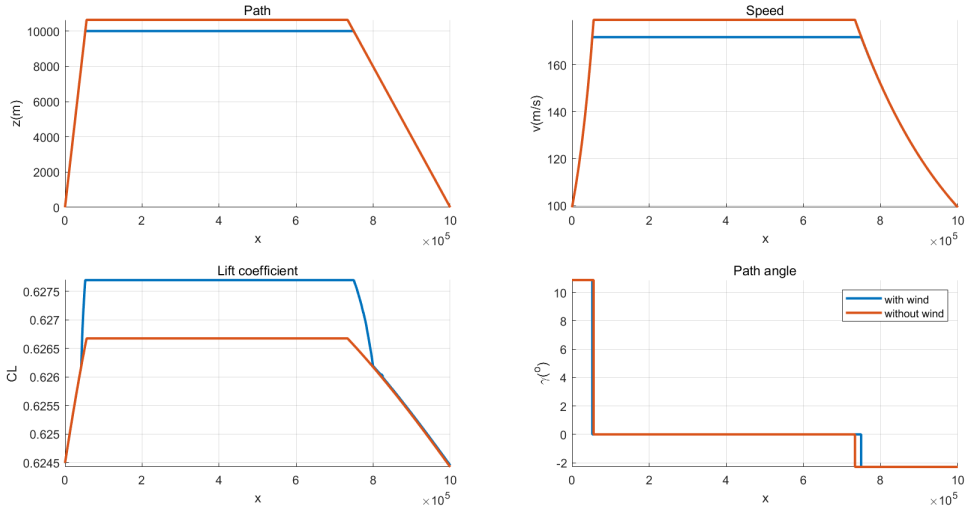

Figure 25: Optimal trajectory with and without wind

Chapter 5

Conclusions

In this thesis, we provided solutions to the optimal flight trajectory in three of the most common Urban Air Mobility (UAM) scenarios. The first problem was the comfort-optimal trajectory for package delivery and passenger transport. The cost was a linear combination of acceleration (or specific support force) and flight time. The solution determined the optimal trajectory in three-dimensional space for arbitrary feasible initial and terminal conditions. An explicit formula for the cost was presented and a peak velocity constraint was enforced. The algorithm can be implemented in common embedded processors since it was designed to use simple calculations no harder than square root and division operations.

The second problem was the control-effort-optimal trajectory for hovering vehicles. Hovering vehicles are expected to be the dominant model of air taxi. The objective function was a linear combination of thrust and flight time. An analytical optimal trajectory was obtained for arbitrary boundary conditions considering linear drag. The approach determined the trajectory for either a fixed time or a free time. An approximate solution was presented for long haul flights to reduce the computational time. A characteristic parameter was proposed to decide whether to use the analytical solution or the approximation. The approach was extended to satisfy peak velocity constraints. To incorporate the wind effect, another result was derived to find the optimal trajectory in a constant wind shear field while respecting peak thrust constraints.

The third problem was the Direct-Operating-Cost (DOC) optimal trajectory for electric fixed-wing aircraft. DOC is a linear combination of energy consumption and flight time. The trajectory planning was formulated as a hybrid optimal control problem (HOCP) to find the optimal trajectory for all phases of a flight. The solution did not require an initial guess of the costate, which saves computational time. A maximum Mach number constraint and a maximum lift coefficient constraint were enforced to prevent solutions that

are practically infeasible. Altitude-dependent along-track horizontal wind was considered so that the solution would be the optimal flight profile in the presence of wind.

Our results for the first two problems are analytical solutions for arbitrary boundary conditions. They can be incorporated with sampling-based methods (such as reference [14]) to interpolate the optimal trajectory between any two adjacent sample points while satisfying additional path constraints. For each solution, we can calculate the expected cost beforehand, which provides a budgeting functionality for all stakeholders. Since our objective functions are a combination of control effort (or specific support force) and flight time, by assigning a different weight to the flight time, we can obtain different trajectories. The effect of the cost index (C_I) is demonstrated. The higher is C_I, the shorter is the flight, which agrees with the fact that time is more expensive. Insight into the cost management of the flight operation industry helps to choose appropriate values for C_I. For the third problem, the optimal flight profile was determined for electric fixed-wing aircraft. We applied the HOC theory to find the optimal flight for all its phases. The effects of four factors were analyzed, namely cost index C_I, efficiency η, mass m, and wind velocity $v_w(z)$. The higher were C_I, η, m, the higher and faster the airplane flew.

Bibliography

[1] NASA. Advanced air mobility (AAM) project. Accessed: 28/05/2020. [Online]. Available: https://nari.arc.nasa.gov/aam

[2] N. Lavars. Autonomous passenger drone swoops onto the flying taxi scene. Accessed: 28/05/2020. [Online]. Available: https://newatlas.com/passenger-drone-flying-taxi/51539

[3] Airbus. E-fan x. Accessed: 28/05/2020. [Online]. Available: https://www.airbus.com/innovation/future-technology/electric-flight/e-fan-x.html

[4] NOAA, "Us standard atmosphere," 1976.

[5] D. P. Thipphavong, R. Apaza, B. Barmore *et al.*, "Urban air mobility airspace integration concepts and considerations," in *2018 Aviation Technology, Integration, and Operations Conference*, Atlanta, Jun 2018, p. 3676.

[6] J. Villarroel, "An optimal control framework for flight management systems," Ph.D. dissertation, Concordia University, 2015.

[7] D. Gallacher, "Drone applications for environmental management in urban spaces: A review," *International Journal of Sustainable Land Use and Urban Planning*, vol. 3, no. 4, 2016.

[8] I. Dayarian, M. Savelsbergh, and J. P. Clarke, "Same-day delivery with drone resupply," *Transportation Science*, Jan 2020.

[9] M. Francisco. (2016, Jul) Organ delivery by 1,000 drones. Accessed: 28/05/2020. [Online]. Available: https://www.nature.com/articles/nbt0716-684a

[10] J. Phillips, "Medical unmanned aerial system for organ transplant delivery," California University of Pennsylvania, Tech. Rep., 2019.

[11] S. Kallas and M. Geoghegan-Quinn, "Flightpath 2050: Europe's vision for aviation: Report of the high level group on aviation research," European Union, Tech. Rep., 2011.

[12] S. A. Viken, F. M. Brooks, and S. C. Johnson, "Overview of the small aircraft transportation system project four enabling operating capabilities," *Journal of aircraft*, vol. 43, no. 6, pp. 1602–1612, 2006.

[13] I. D. Jacobson and L. G. Richards, "Ride quality evaluation II: modelling of airline passenger comfort," *Ergonomics*, vol. 19, no. 1, pp. 1–10, 1976.

[14] P. Pharpatara, B. Hérissé, and Y. Bestaoui, "3-D trajectory planning of aerial vehicles using RRT," *IEEE Transactions on Control Systems Technology*, vol. 25, no. 3, pp. 1116–1123, 2016.

[15] F. Patrón, R. Salvador, and R. M. Botez, "Flight trajectory optimization through genetic algorithms coupling vertical and lateral profiles," in *Proceedings of ASME 2014 International Mechanical Engineering Congress and Exposition*, Nov 2014.

[16] I. Lugo-Cárdenas, G. Flores, S. Salazar, and R. Lozano, "Dubins path generation for a fixed wing UAV," in *Proceedings of 2014 International conference on unmanned aircraft systems (ICUAS)*. IEEE, 2014, pp. 339–346.

[17] E. S. Palacios and M. A. Johnson, "4D BADA-based trajectory generator and 3D guidance algorithm," in *Mexican Society of Science and Aerospace*. Baja California: NASA, Sep 2013. [Online]. Available: https://ntrs.nasa.gov/search.jsp?R=20140008892

[18] S. Kumakshev and A. Shmatkov, "Flight trajectory optimization without decomposition into separate stages," in *IOP Conference Series: Materials Science and Engineering*, vol. 468, no. 1. IOP Publishing, 2018, p. 012033.

[19] M. Kaptsov and L. Rodrigues, "Flight management systems for all-electric aircraft," in *Proceedings of 2017 IEEE Conference on Control Technology and Applications (CCTA)*. IEEE, 2017, pp. 2126–2131.

[20] R. Ritz, M. Hehn, S. Lupashin, and R. D'Andrea, "Quadrocopter performance benchmarking using optimal control," in *2011 IEEE/RSJ International Conference on Intelligent Robots and Systems*. IEEE, 2011, pp. 5179–5186.

[21] Y. Bouktir, M. Haddad, and T. Chettibi, "Trajectory planning for a quadrotor helicopter," in *2008 16th mediterranean conference on control and automation*. IEEE, 2008, pp. 1258–1263.

[22] E. Kahale, P. Castillo, and Y. Bestaoui, "Minimum time reference trajectory generation for an autonomous quadrotor," in *2014 International Conference on Unmanned Aircraft Systems (ICUAS)*. IEEE, 2014, pp. 126–133.

[23] F. Morbidi, R. Cano, and D. Lara, "Minimum-energy path generation for a quadrotor UAV," in *2016 IEEE International Conference on Robotics and Automation (ICRA)*. IEEE, 2016, pp. 1492–1498.

[24] B. Carvalho, M. Di Perna, and L. Rodrigues, "Real-time optimal trajectory generation for a quadrotor UAV on the longitudinal plane," in *2018 European Control Conference (ECC)*. IEEE, 2018, pp. 3132–3136.

[25] B. Pereira de Carvalho, "A framework for energy efficient UAV trajectory planning," Ph.D. dissertation, Concordia University, 2018.

[26] R. L. Schultz and N. R. Zagalsky, "Aircraft performance optimization." *Journal of Aircraft*, vol. 9, no. 2, pp. 108–114, 1972.

[27] M. Hehn and R. D'Andrea, "Quadrocopter trajectory generation and control," *IFAC proceedings Volumes*, vol. 44, no. 1, pp. 1485–1491, 2011.

[28] D. Mellinger and V. Kumar, "Minimum snap trajectory generation and control for quadrotors," in *2011 IEEE International Conference on Robotics and Automation*. IEEE, 2011, pp. 2520–2525.

[29] B. Carvalho and L. Rodrigues, "Optimal longitudinal trajectory planning for a quadrotor UAV including linear drag effects," in *2019 18th European Control Conference (ECC)*. IEEE, 2019, pp. 2689–2694.

[30] A. Taitler, I. Ioslovich, P.-O. Gutman, and E. Karpas, "Combined time and energy optimal trajectory planning with quadratic drag for mixed discrete-continuous task planning," *Optimization*, vol. 68, no. 1, pp. 125–143, 2019.

[31] A. Chakravarty, "Four-dimensional fuel-optimal guidance in the presence of winds," *Journal of Guidance, Control, and Dynamics*, vol. 8, no. 1, pp. 16–22, 1985.

[32] M. R. Jardin and A. E. Bryson Jr, "Neighboring optimal aircraft guidance in winds," *Journal of Guidance, Control, and Dynamics*, vol. 24, no. 4, pp. 710–715, 2001.

[33] H. K. Ng, B. Sridhar, and S. Grabbe, "A practical approach for optimizing aircraft trajectories in winds," in *2012 IEEE/AIAA 31st Digital Avionics Systems Conference (DASC)*. IEEE, 2012, pp. 3D6–1.

[34] X. Chu, X. Lin, and W. Lan, "Energy-optimal rectilinear trajectory for stratospheric airships in constant wind field," in *2013 IEEE International Conference on Cyber Technology in Automation, Control and Intelligent Systems*. IEEE, 2013, pp. 264–269.

[35] J. Zillies, A. Kuenz, A. Schmitt, G. Schwoch, V. Mollwitz, and C. Edinger, "Wind optimized routing: An opportunity to improve European flight efficiency?" in *2014 Integrated Communications, Navigation and Surveillance Conference (ICNS) Conference Proceedings*. IEEE, 2014, pp. X3–1.

[36] O. Rodionova, M. Sbihi, D. Delahaye, and M. Mongeau, "North Atlantic aircraft trajectory optimization," *IEEE Transactions on Intelligent Transportation Systems*, vol. 15, no. 5, pp. 2202–2212, 2014.

[37] M. Brown, H. Hirabayshi, and N. K. Wickramasinghe, "A graph search-based trajectory optimiser for practical wind-optimal trajectories," in *Asia-Pacific International Symposium on Aerospace Technology*. Springer, 2018, pp. 2201–2208.

[38] S. Schopferer and T. Pfeifer, "Performance-aware flight path planning for unmanned aircraft in uniform wind fields," in *2015 International Conference on Unmanned Aircraft Systems (ICUAS)*. IEEE, 2015, pp. 1138–1147.

[39] A. Murrieta-Mendoza, B. Beuze, L. Ternisien, and R. M. Botez, "New reference trajectory optimization algorithm for a flight management system inspired in beam search," *Chinese Journal of Aeronautics*, vol. 30, no. 4, pp. 1459–1472, 2017.

[40] R. S. Félix Patrón, M. Schindler, and R. M. Botez, "Aircraft trajectories optimization by genetic algorithms to reduce flight cost using a dynamic weather model," in *15th AIAA Aviation Technology, Integration, and Operations Conference*. AIAA, 2015, p. 2281.

[41] C. Currie, A. Marcos, and O. Turnbull, "Wind optimal flight trajectories to minimise fuel consumption within a 3 dimensional flight network," in *2016 UKACC 11th International Conference on Control (CONTROL)*. IEEE, 2016, pp. 1–6.

[42] S. G. Park and J. P. Clarke, "Vertical trajectory optimization to minimize environmental impact in the presence of wind," *Journal of Aircraft*, vol. 53, no. 3, pp. 725–737, 2016.

[43] A. Valenzuela and D. Rivas, "Analysis of along-track variable wind effects on optimal aircraft trajectory generation," *Journal of Guidance, Control, and Dynamics*, pp. 2149–2156, 2016.

[44] I. Dhief, N. H. Dougui, D. Delahaye, and N. Hamdi, "A new trans-Atlantic route structure for strategic flight planning over the NAT airspace," in *2017 IEEE Congress on Evolutionary Computation (CEC)*. IEEE, 2017, pp. 1511–1518.

[45] Z. Liu, A. Kurzhanskiy, and R. Sengupta, "An energy-based optimal control problem for unmanned aircraft systems flight planning," in *2017 56th Annual Conference of the Society of Instrument and Control Engineers of Japan (SICE)*. IEEE, 2017, pp. 1320–1325.

[46] J. A. Guerrero, J. A. Escareño, and Y. Bestaoui, "Quad-rotor mav trajectory planning in wind fields," in *2013 IEEE International Conference on Robotics and Automation*. IEEE, 2013, pp. 778–783.

[47] J. P. Silva, C. de Wagter, and G. de Croon, "Quadrotor thrust vectoring control with time and jerk optimal trajectory planning in constant wind fields," *Unmanned Systems*, vol. 6, no. 01, pp. 15–37, 2018.

[48] S. Torres and J. Dehn, "Wind optimal trajectories for UAS and light aircraft," in *2017 IEEE/AIAA 36th Digital Avionics Systems Conference (DASC)*. IEEE, 2017, pp. 1–8.

[49] K. Legrand, S. Puechmorel, D. Delahaye, and Y. Zhu, "Robust aircraft optimal trajectory in the presence of wind," *IEEE Aerospace and Electronic Systems Magazine*, vol. 33, no. 11, pp. 30–38, 2018.

[50] R. A. Altava, J. C. Mere, D. Delahaye, and T. Miquel, "Flight management system pathfinding algorithm for automatic vertical trajectory generation," in *2018 IEEE/AIAA 37th Digital Avionics Systems Conference (DASC)*. IEEE, 2018, pp. 1–9.

[51] A. Alizadeh, M. Uzun, E. Koyuncu, and G. Inalhan, "Optimal en-route trajectory planning based on wind information," *IFAC-PapersOnLine*, vol. 51, no. 9, pp. 180–185, 2018.

[52] J. Xiang, T. Shen, and D. Li, "Trajectory planning for mini unmanned helicopter in obstacle and windy environments," *Aircraft Engineering and Aerospace Technology*, vol. 90, no. 5, pp. 806–814, 2018.

[53] L. Juve, J. Fosse, E. Joubert, and N. Fouquet, "Airbus group electrical aircraft program, the E-Fan project," in *52nd AIAA/SAE/ASEE Joint Propulsion Conference*, Salt lake city, Jul 2016, p. 4613.

[54] ICAO, "9613 an/937, performance—based navigation (pbn) manual," ICAO, Tech. Rep.

[55] A. Gardi, R. Sabatini, and S. Ramasamy, "Multi-objective optimisation of aircraft flight trajectories in the atm and avionics context," *Progress in Aerospace Sciences*, vol. 83, pp. 1–36, 2016.

[56] P. K. Menon and S. Park, "Dynamics and control technologies in air traffic management," *Annual Reviews in Control*, vol. 42, pp. 271–284, 2016.

[57] A. W. Hammad, D. Rey, A. Bu-Qammaz, H. Grzybowska, and A. Akbarnezhad, "Mathematical optimization in enhancing the sustainability of aircraft trajectory: A review," *International Journal of Sustainable Transportation*, pp. 1–24, 2019.

[58] A. E. Bryson Jr, M. N. Desai, and W. C. Hoffman, "Energy-state approximation in performance optimization of supersonic aircraft," *Journal of Aircraft*, vol. 6, no. 6, pp. 481–488, 1969.

[59] J. F. Barman and H. Erzberger, "Fixed-range optimum trajectories for short-haul aircraft," *Journal of Aircraft*, vol. 13, no. 10, pp. 748–754, 1976.

[60] J. A. Sorensen, S. A. Morello, and H. Erzberger, "Application of trajectory optimization principles to minimize aircraft operating costs," in *1979 18th IEEE Conference on Decision and Control including the Symposium on Adaptive Processes*, vol. 2. IEEE, 1979, pp. 415–421.

[61] H. Erzberger and H. Lee, "Constrained optimum trajectories with specified range," *Journal of Guidance and Control*, vol. 3, no. 1, pp. 78–85, 1980.

[62] J. W. Burrows, "Fuel optimal trajectory computation," *Journal of Aircraft*, vol. 19, no. 4, pp. 324–329, 1982.

[63] F. Neuman and E. Kreindler, "Minimum-fuel, three-dimensional flight paths for jet transports," *Journal of Guidance, Control, and Dynamics*, vol. 8, no. 5, pp. 650–657, 1985.

[64] M. Kaptsov, "An energy efficient optimal control framework for general purpose flight management systems," Ph.D. dissertation, Concordia University, 2017.

[65] M. Soler, A. Olivares, and E. Staffetti, "Hybrid optimal control approach to commercial aircraft trajectory planning," *Journal of Guidance, Control, and Dynamics*, vol. 33, no. 3, pp. 985–991, 2010.

[66] ——, "Multiphase optimal control framework for commercial aircraft four-dimensional flight-planning problems," *Journal of Aircraft*, vol. 52, no. 1, pp. 274–286, 2015.

[67] A. Gardi, R. Sabatini, and T. Kistan, "Multiobjective 4D trajectory optimization for integrated avionics and air traffic management systems," *IEEE Transactions on Aerospace and Electronic Systems*, vol. 55, no. 1, pp. 170–181, 2018.

[68] C. R. Hargraves and S. W. Paris, "Direct trajectory optimization using nonlinear programming and collocation," *Journal of guidance, control, and dynamics*, vol. 10, no. 4, pp. 338–342, 1987.

[69] G. T. Huntington and A. V. Rao, "A comparison between global and local orthogonal collocation methods for solving optimal control problems," in *2007 American Control Conference*. IEEE, 2007, pp. 1950–1957.

[70] R. S. F. Patrón, Y. Berrou, and R. M. Botez, "New methods of optimization of the flight profiles for performance database-modeled aircraft," *Proceedings of the Institution of Mechanical Engineers, Part G: Journal of Aerospace Engineering*, vol. 229, no. 10, pp. 1853–1867, 2015.

[71] A. Franco and D. Rivas, "Optimization of multiphase aircraft trajectories using hybrid optimal control," *Journal of Guidance, Control, and Dynamics*, vol. 38, no. 3, pp. 452–467, 2015.

[72] Y. Zhao and P. Tsiotras, "Time-optimal parameterization of geometric path for fixed-wing aircraft," in *AIAA Infotech@ Aerospace 2010*, 2010, p. 3352.

[73] D. Liberzon, *Calculus of variations and optimal control theory: a concise introduction*. Princeton University Press, 2011.

[74] L. S. Pontryagin, *Mathematical theory of optimal processes*. Routledge, 2018.

[75] J. D. Hoffman and S. Frankel, *Numerical methods for engineers and scientists*. CRC press, 2018.

[76] P. Jarratt, "An iterative method for locating turning points," *The Computer Journal*, vol. 10, no. 1, pp. 82–84, 1967.

[77] J. P. Owen and W. S. Ryu, "The effects of linear and quadratic drag on falling spheres: an undergraduate laboratory," *European Journal of Physics*, vol. 26, no. 6, p. 1085, 2005.

[78] DJI. (2018) Phantom 4 pro. Accessed: 28/05/2020. [Online]. Available: https://www.dji.com/ca/phantom-4-pro/info

[79] E. V. News. (2018) Sikorsky firefly. Accessed: 28/05/2020. [Online]. Available: http://evtol.news/aircraft/sikorsky-firefly/

[80] J. Roskam, *Airplane flight dynamics and automatic flight controls*. DARcorporation, 1998.

[81] M. Cavcar, "The international standard atmosphere (ISA)," Anadolu University, Turkey, Tech. Rep. 9, 2000.

[82] A. Pakniyat and P. E. Caines, "On the relation between the minimum principle and dynamic programming for classical and hybrid control systems," *IEEE Transactions on Automatic Control*, vol. 62, no. 9, pp. 4347–4362, 2017.

[83] A. Nuic, *User Manual for the Base of Aircraft Data (BADA) Revision 3.12*, EUROCONTROL Experimental Centre, EET Technical, 2014.